John Barnard
Steven Lund
USPAS
June 2006

An application of intense beams

1. Heavy-ion fusion
   A. Requirements
   B. Targets for ICF
   C. Accelerator
   D. Drift compression
   E. Final focus
   F. Experiments

Inertial Fusion Energy (IFE) power plants of the future will consist of four parts

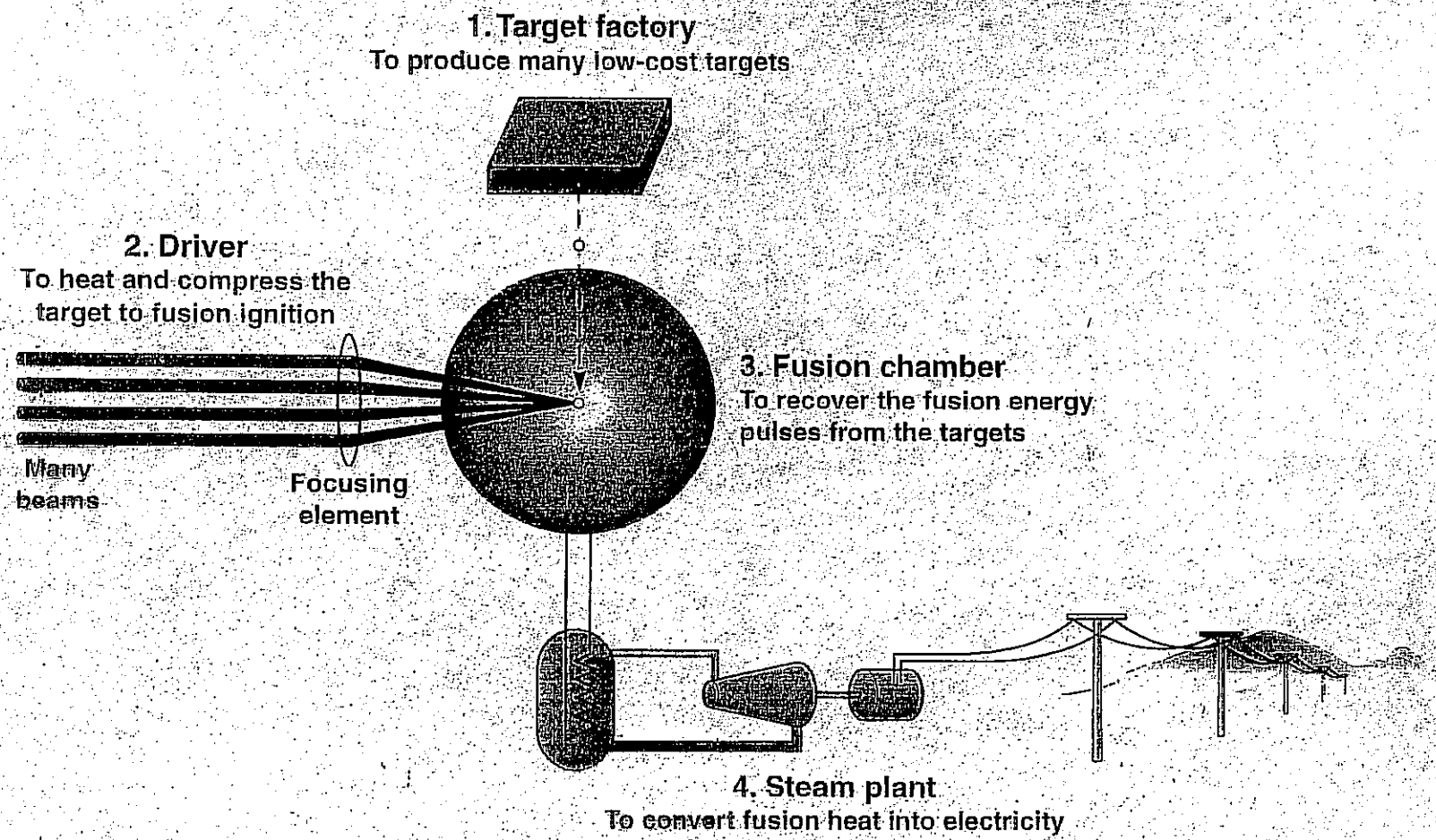

A power-plant driver would fire about five targets per second to produce as much electricity as today's 1000-megawatt power plant

05-00-0396-0609
2fRWM/mcm

8/26/96

2

Heavy Ion Fusion provides an attractive approach to long term energy production

Fusion offers an inexaustible, long term solution to the problem of future energy supplies free from long-lived radioactive by-products and greenhouse CO_2.

Inertial Confinement Fusion (ICF) uses laser or particle beams to implode a target, raising the temperature and density of the fuel, creating the conditions necessary for the following reaction:

$$D + T \rightarrow n\ (14.06\ MeV) + He^4\ (3.52\ MeV)\ .$$

Heavy ion accelerators are a strong candidate for inertial fusion *energy production* (IFE) because of:

- High efficiency
- High repetition rate
- Survivability of final lens
- Favorable target illumination geometry

Focusability at the target is key scientific issue

Conditions of beam at target are set by hohlraum and implosion physics

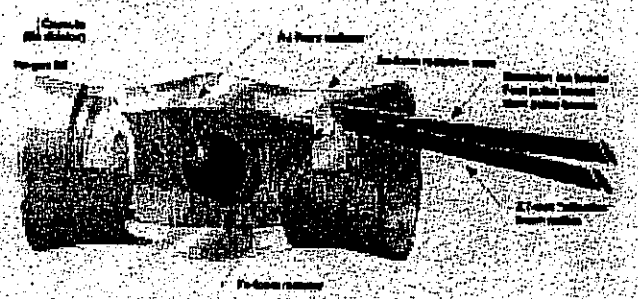

Energy in pulse: ~ 3 to 6 MJ

Duration of main pulse: ~ 8 to 10 ns

Duration of foot pulse: ~ 30 ns

Spot radius: ~ 1.5 to 3 mm

Transverse and longitudinal compression are required to meet target specifications.

Length of beam just outside of injector ~25-50 m

At target ~ 0.5 - 1 m

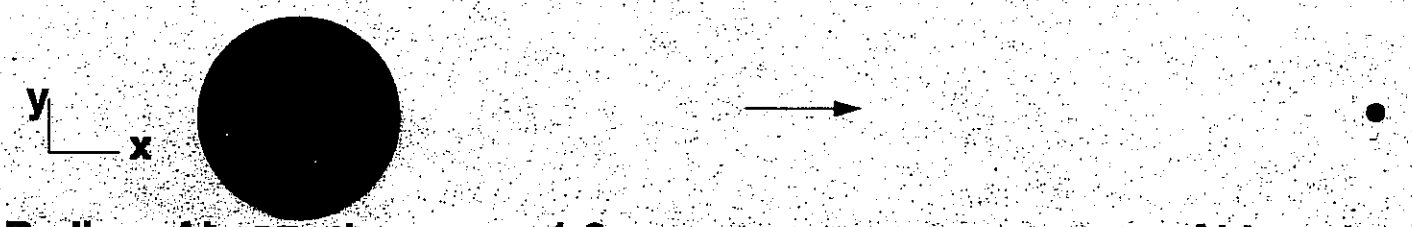

Radius of beam at source ~ 1-3 cm

At target ~ 1.5-3 mm

Compression factors of 10 to 50 in both longitudinal and transverse directions are required.

A "DISTRIBUTED RADIATOR" TARGET PRODUCES HIGH GAIN IN RADIATION—HYDRODYNAMIC SIMULATIONS

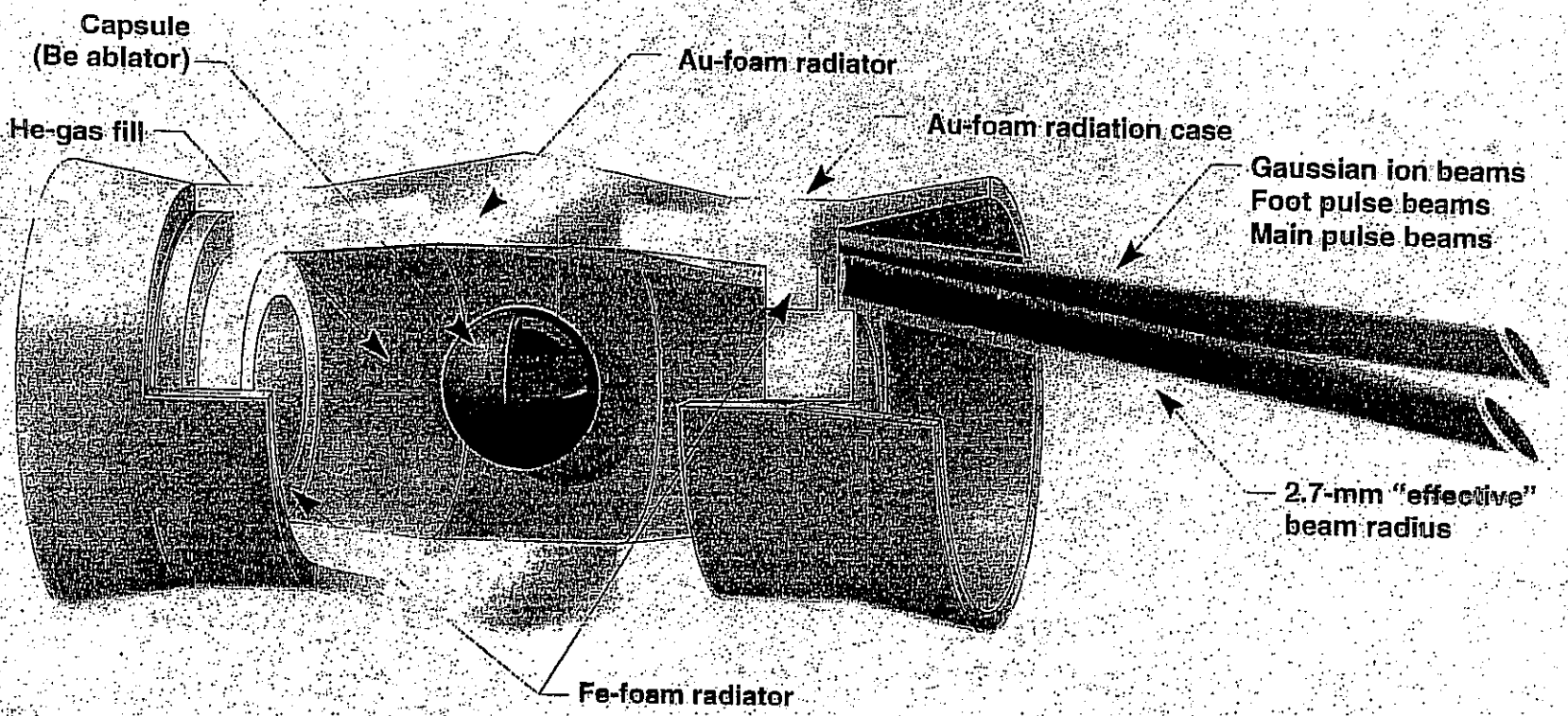

05-00-0998-1862A
sJDL/cld

9/10/98

The two principal approaches to ICF are direct drive and indirect drive

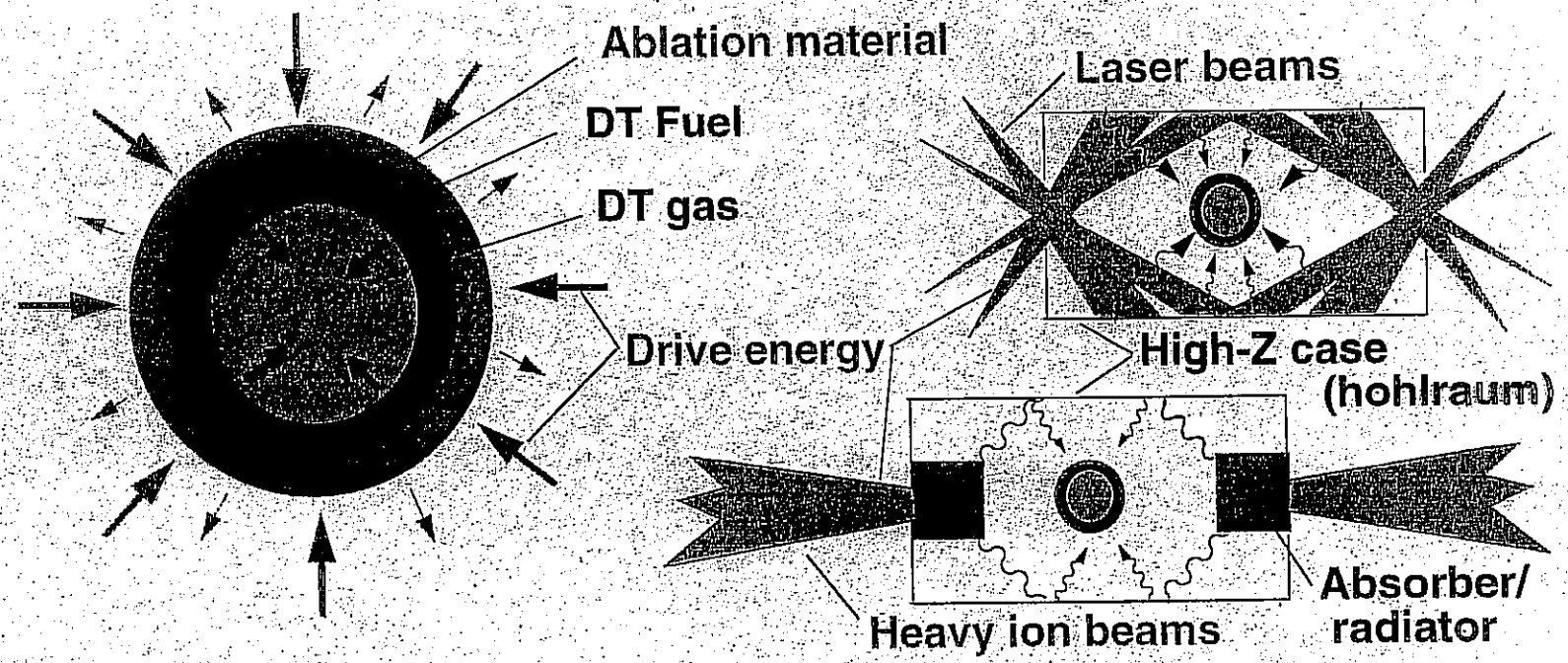

Direct drive:

Advantage:

- Higher coupling efficiency (with potential for higher gain)

Indirect drive:

Advantages:

- Relaxed beam uniformity (reduced hydro instability)
- Significant commonality for lasers and ion beams
- Significant simplification of chamber geometry

National Ignition Facility has 192 beams of 40-cm aperture arranged in four beam clusters

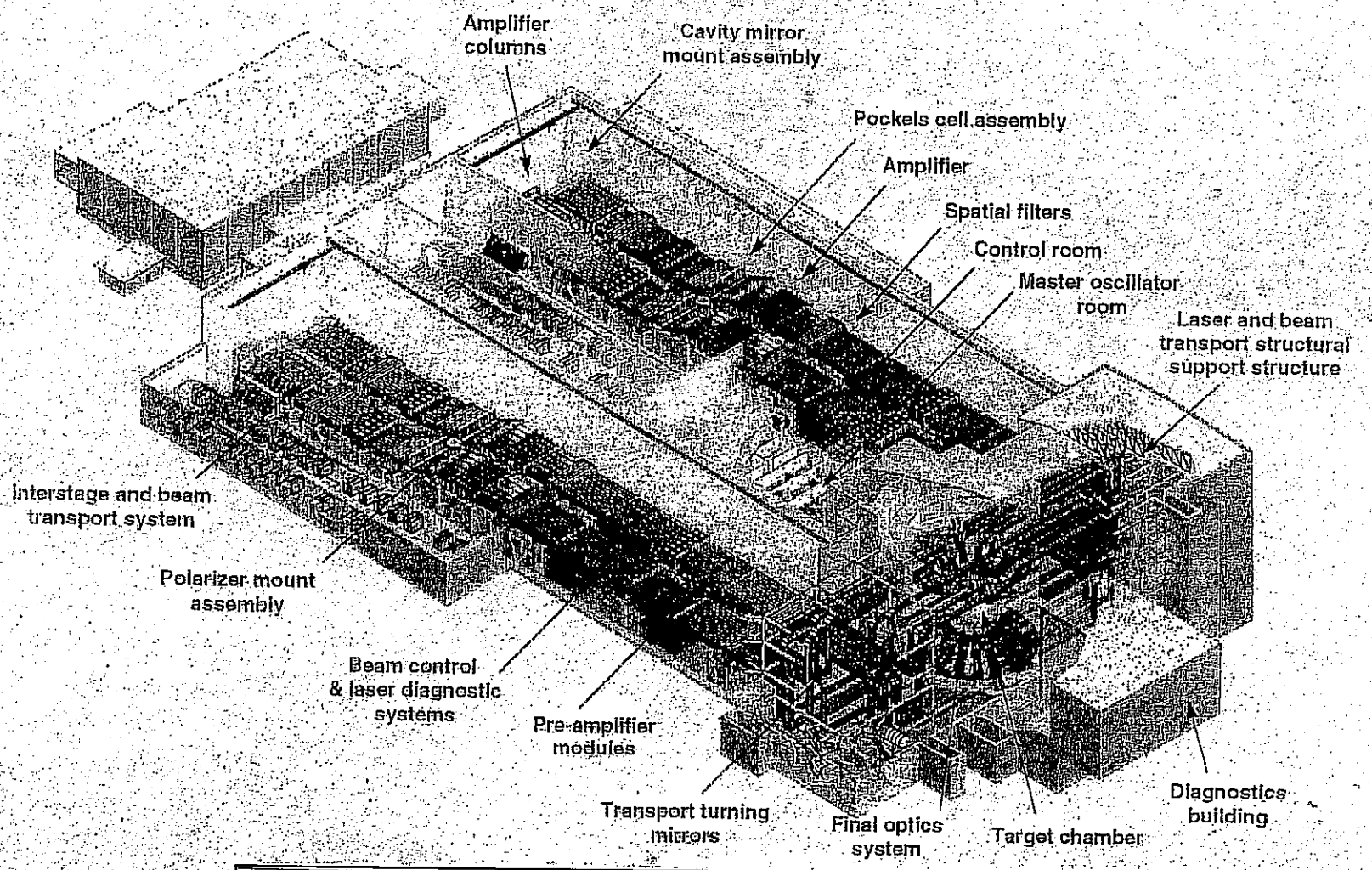

NIF illustrates many of the features of IFE development and will play a critical role in addressing IFE feasibility

40-00-0996-2100YA
03GAD/gbh

5/1/98
BMC/jco

7

Ion current profile and radiation temperature

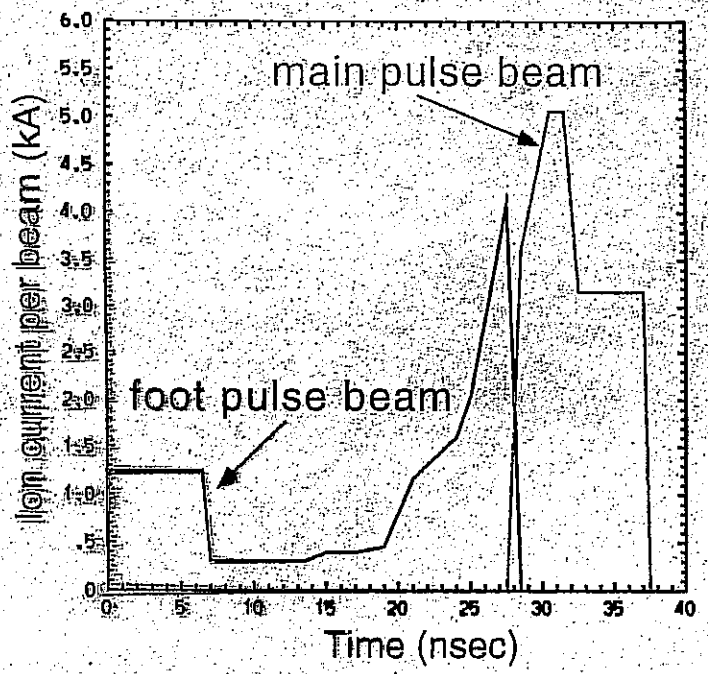

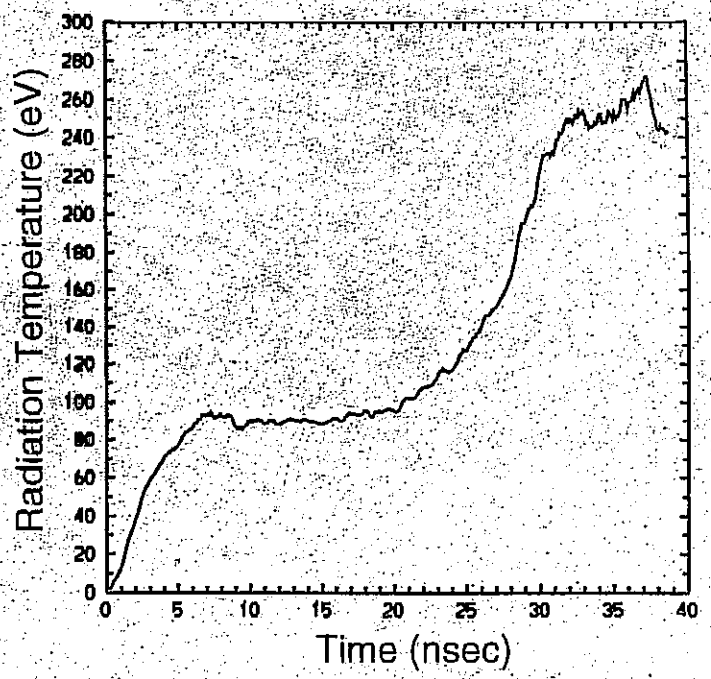

Current assumes 16 beams in foot pulse
32 beams in main pulse

Callahan 11/97

Overlapping Gaussian, elliptical beams are focused at the end of the target

Each beam is an ellipse

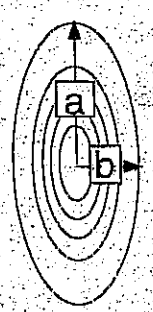

8 beams overlap in the foot pulse

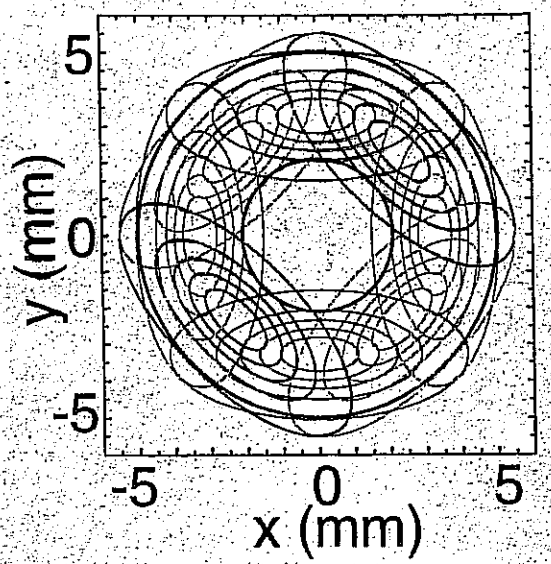

Sum of 8 foot pulse beams

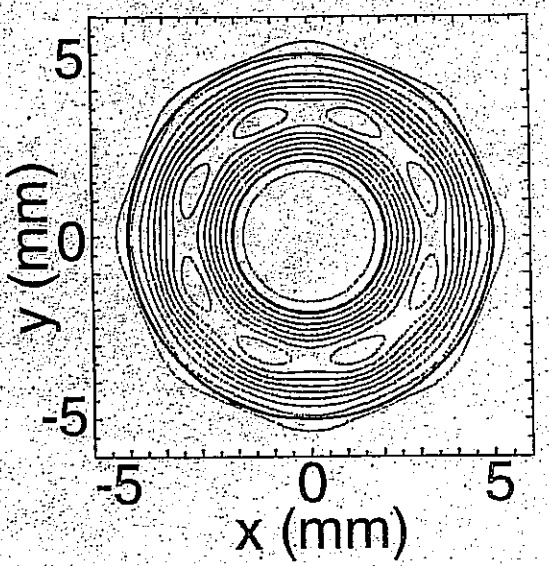

a = 4.15 mm
b = 1.8 mm
effective r=2.7 mm
95% of charge inside

Azimuthal asymmetry:
foot pulse: -1.6% in m=8
main pulse: 0.06% in m=16

Callahan 8/97

Why Heavy Ions?

Target requires:

3.5 - 6 MJ in ~ 10 ns ⇒ ~ 500 TW = I · V

Range ~ 0.02 - .2 g/cm²

qV = kinetic energy

I = current

Range requirement → Higher mass ⇔ higher kinetic energy

Power Requirement → Current ∝ $\frac{1}{\text{kinetic energy}}$

Higher mass requires lower current (easier to focus).

5

Heavier Ions ⇒ Higher Kinetic Energy

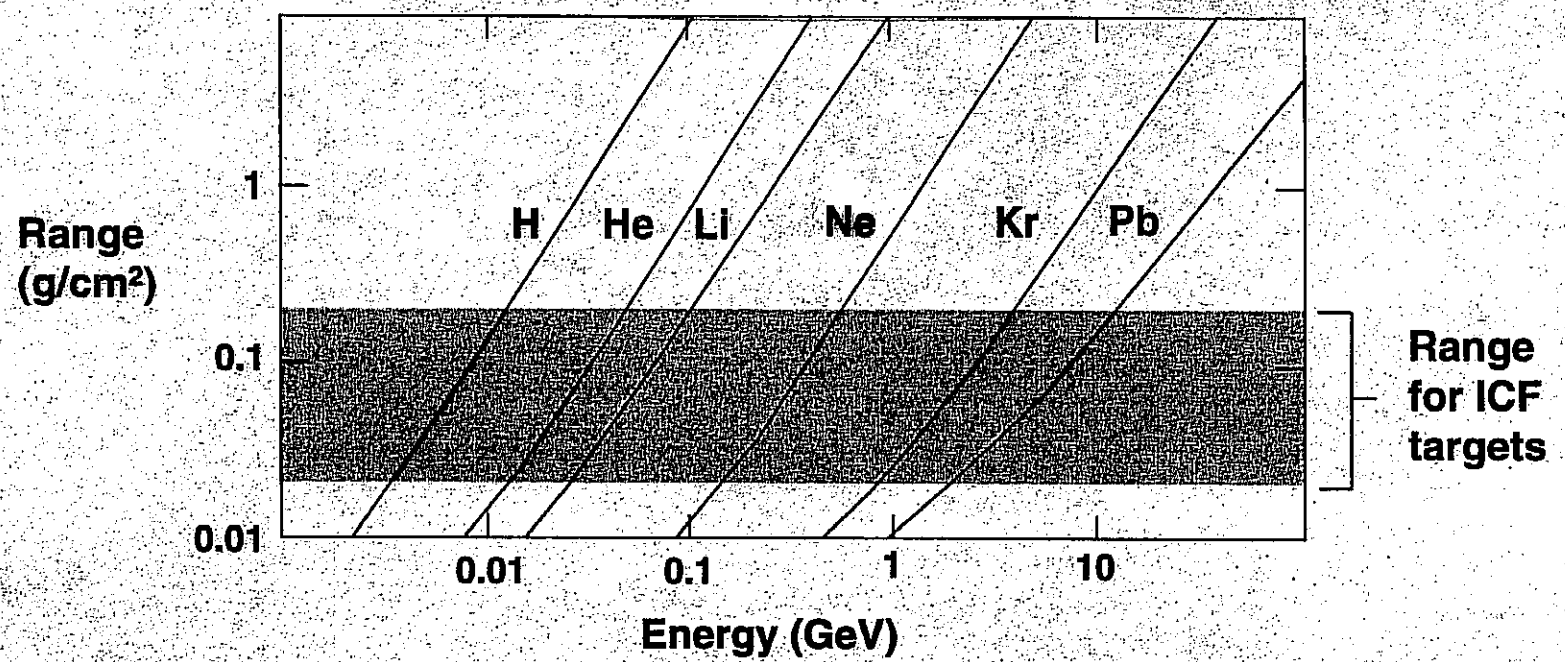

Targets require high power (kinetic energy x current).

- Light Ion Fusion requires high-current, unconventional accelerators (Sandia 1970s).
- Heavy Ion Fusion requires lower currents enabling the use of more conventional high energy accelerators (Maschke ~ 1974).

There are two principle methods of acceleration

1. r.f. acceleration
(Approach in Europe and Japan)

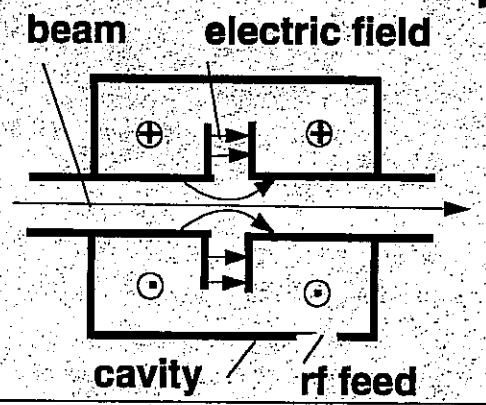

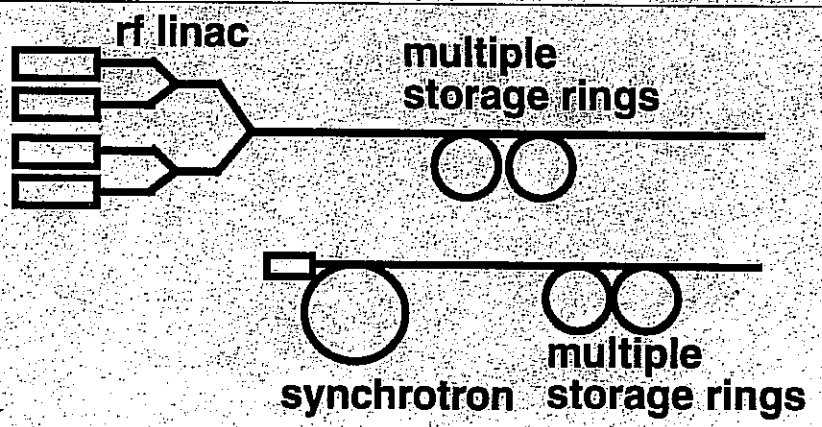

2. Induction acceleration
(U.S. approach)

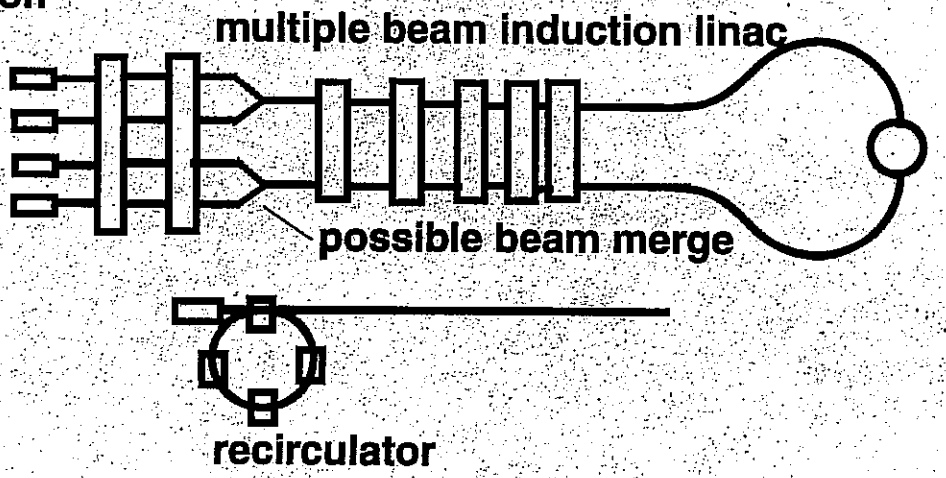

Induction acceleration for HIF consists of several subsystems and a variety of beam manipulations

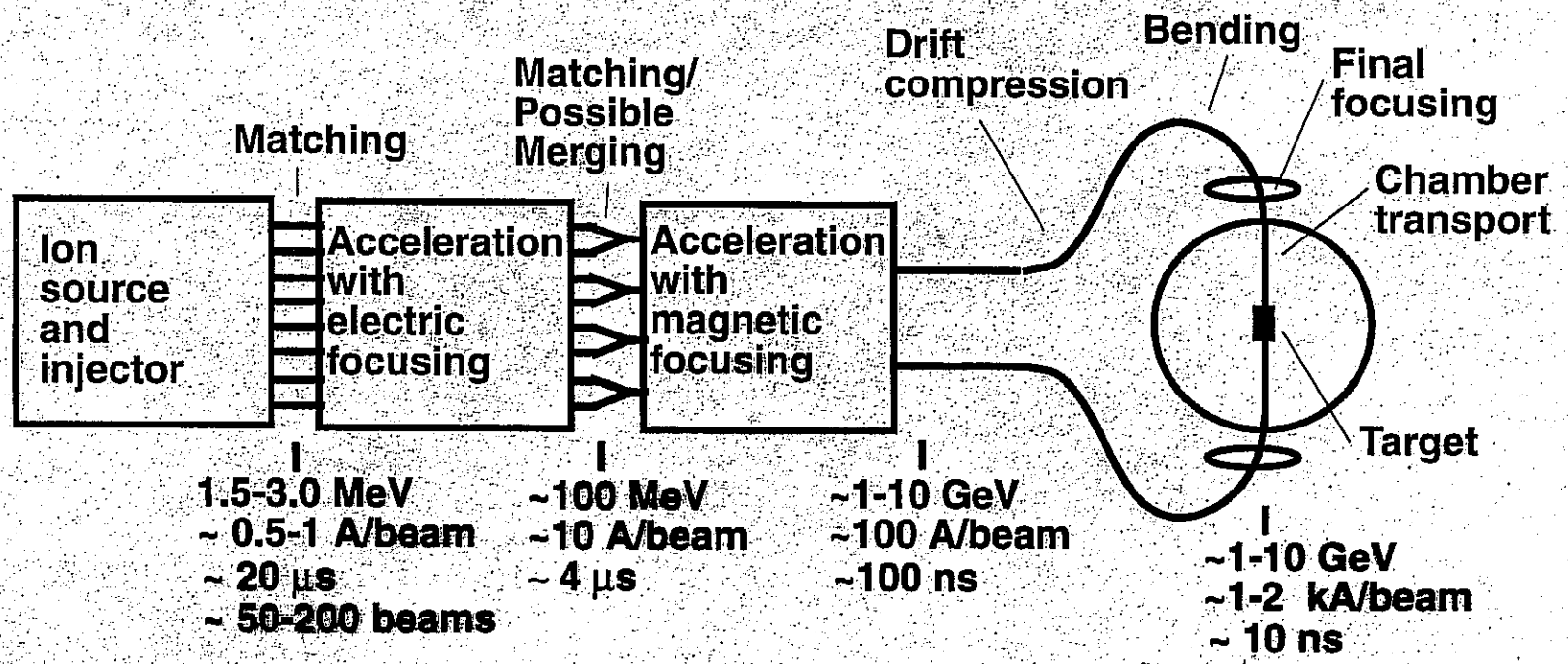

A Robust Point Design study established a baseline for a multiple-beam quadrupole induction linac HIF driver

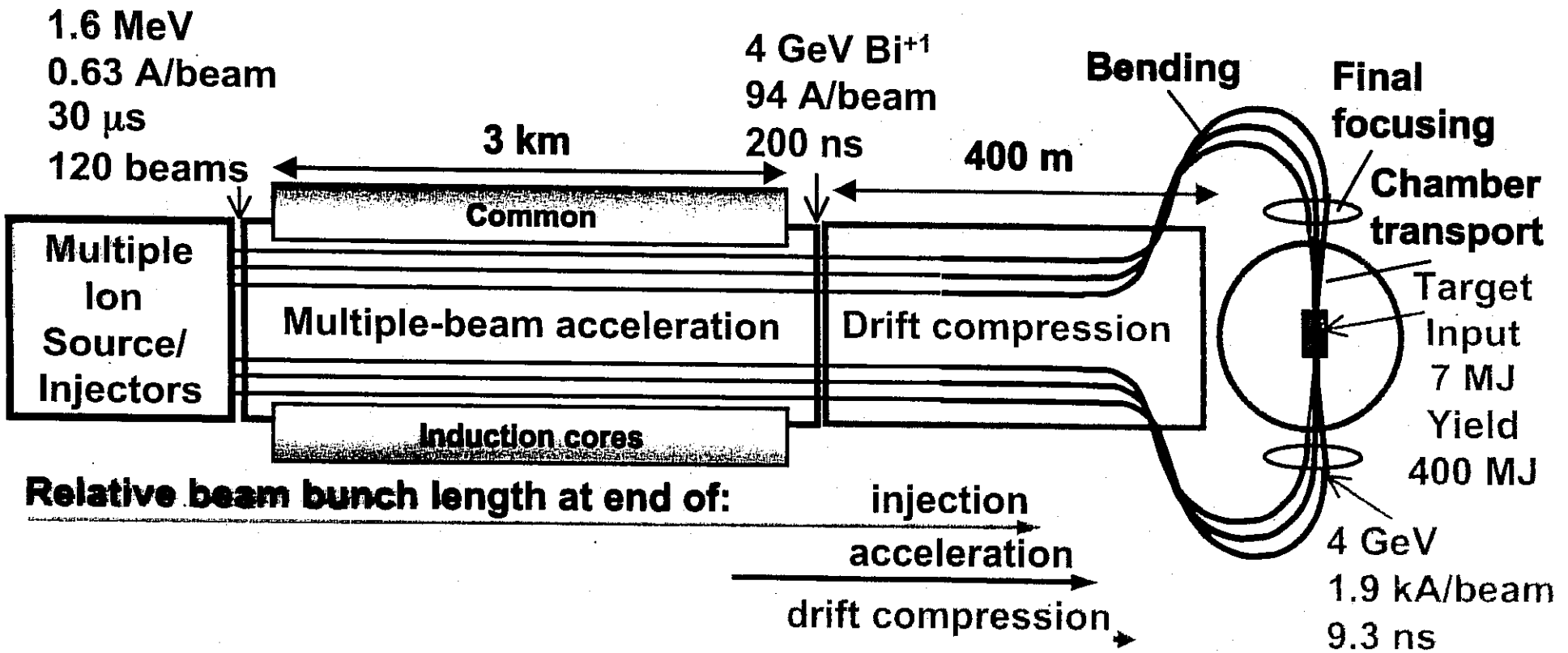

Major components of an induction linac

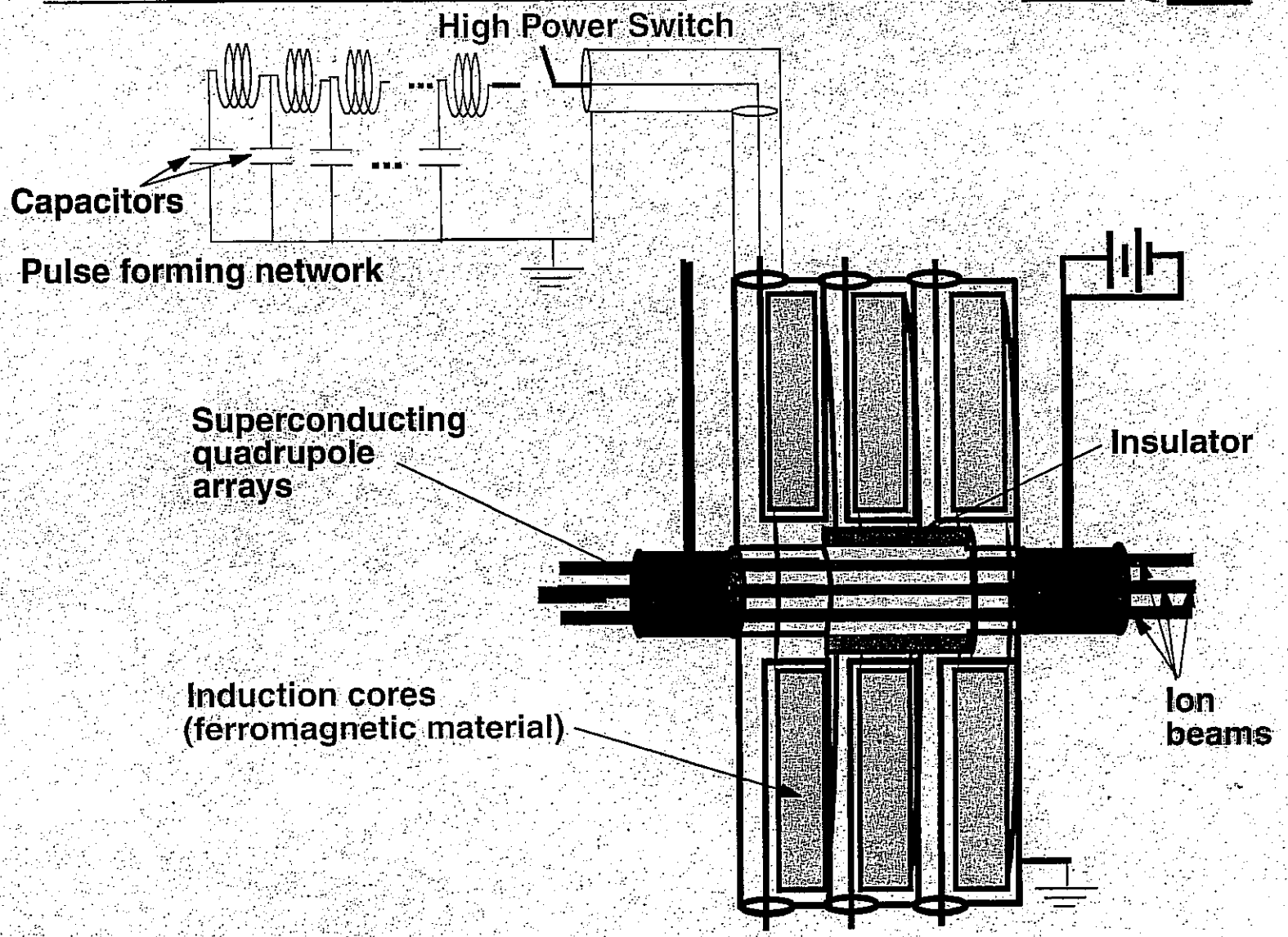

An Induction Core

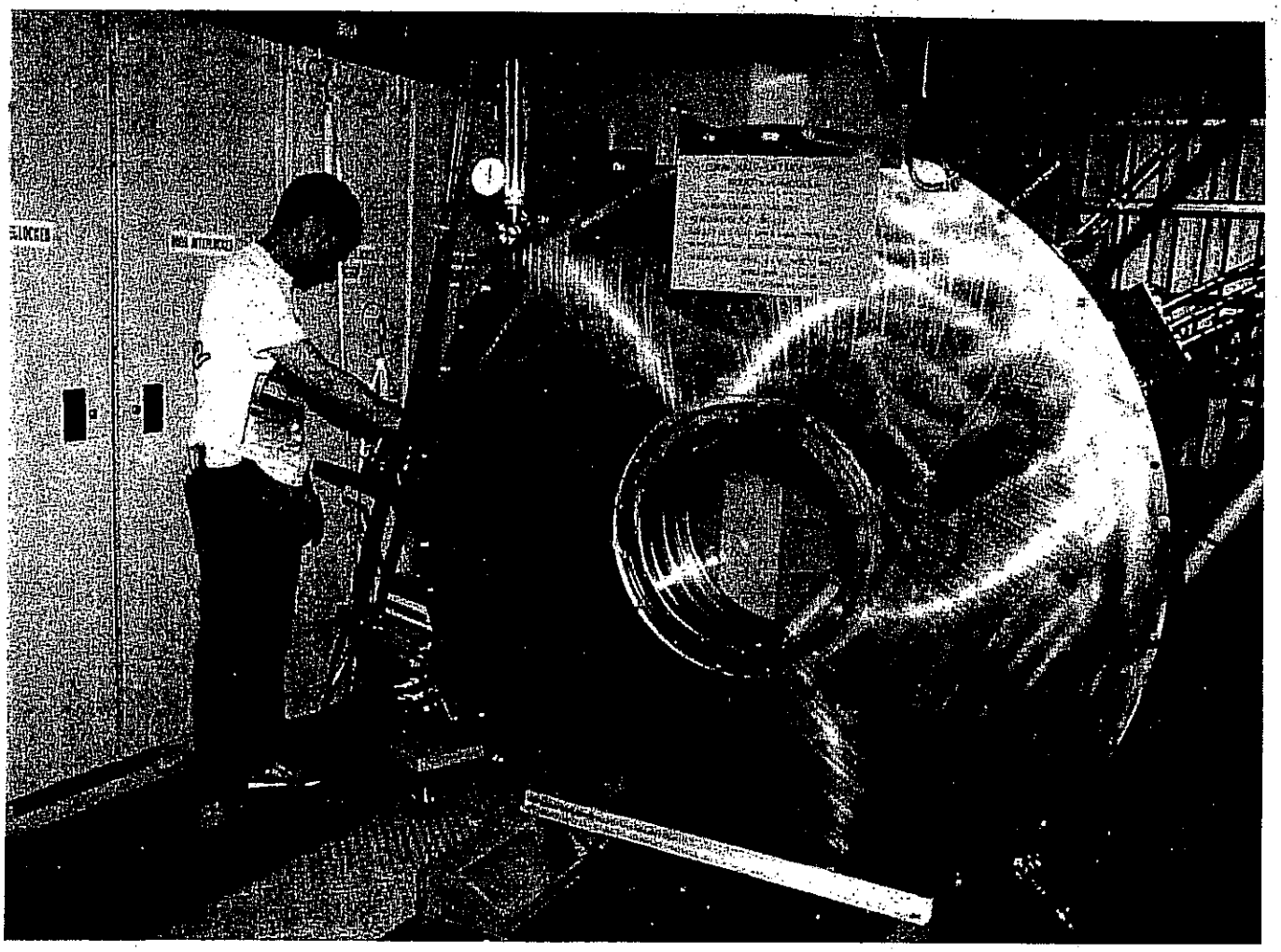

An array of small beamlets increases the total beam current through the core

From class:

$$\frac{Q}{a} = \left(\frac{\sigma_0^2}{4L^2}\right) a$$

$$\sigma_0 \cong \frac{4L^2}{[B_\rho]} B'$$

$$I \sim \beta^3 Q$$

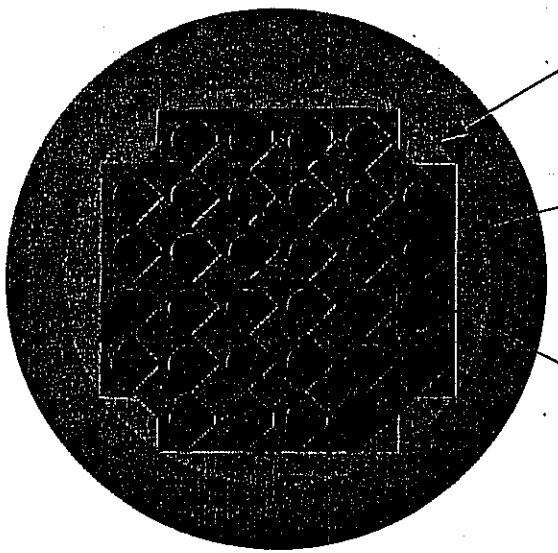

Core (radius = R_{core})

Multibeam quad array

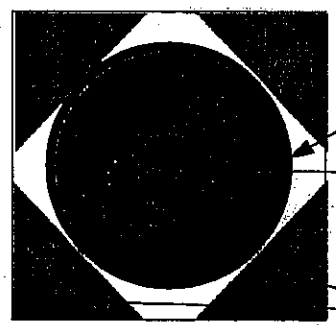

beam pipe (radius = r_p)

beam (radius = a)

quadrupole magnet winding

Current per beam = $I_b \sim a^2 B \beta^2/r_p$

$r_p \sim a$ (until misalignments require minimum size--better: $r_p = c_1 a + c_2$)

so $I_b \sim a$; N_b = number of beams in array $\sim R^2_{core} / a^2$

Total current through core = $I_{tot} = N_b I_b \sim R^2_{core} / a$ (until misalignments dominate scaling)

A Typical driver has about 2000 individual modules

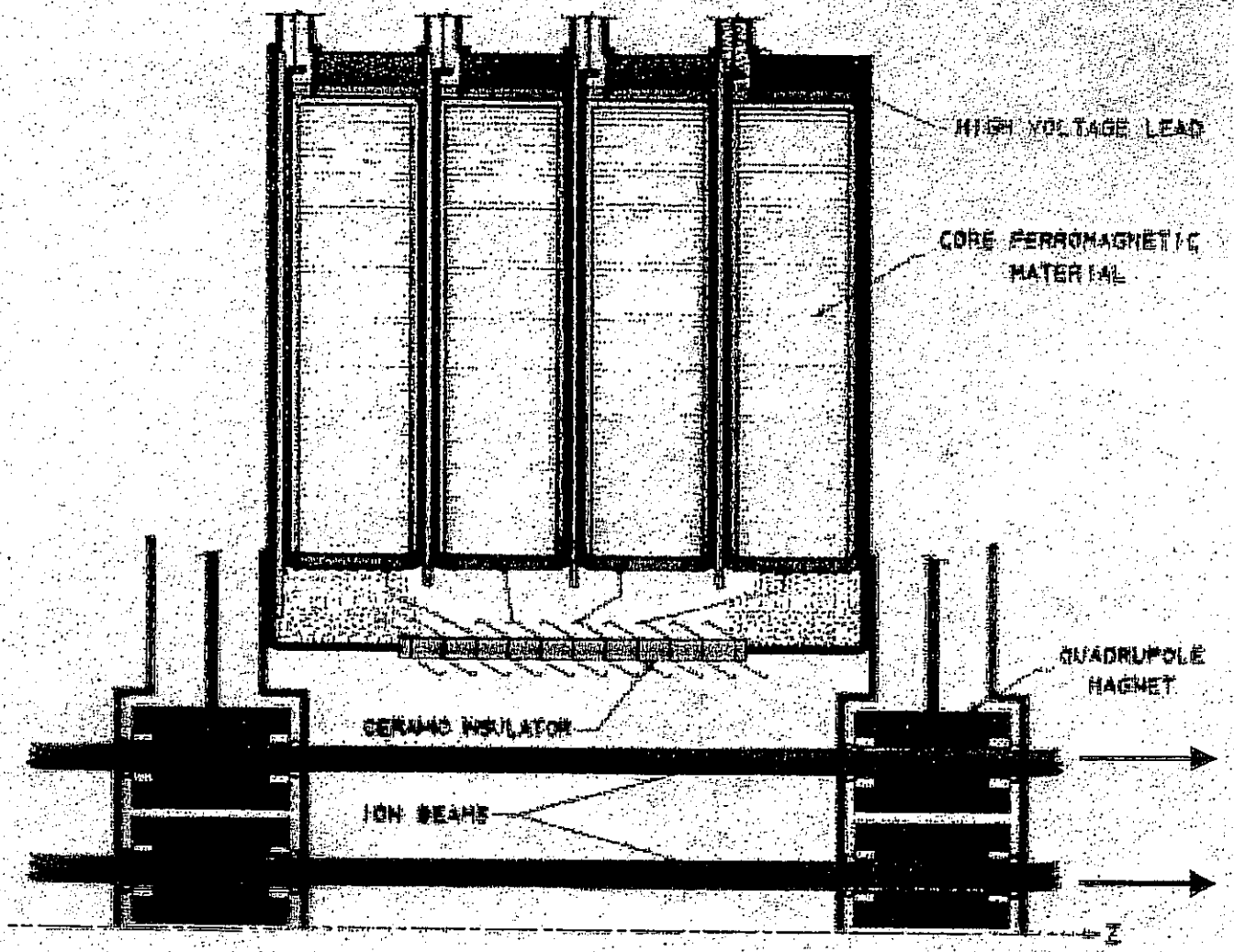

In an induction linac, certain limits constrain design

Phase advance per lattice period $\sigma_0 < \sim 85^o$ **(to avoid envelope/lattice instabilities** & emittance growth).

Space charge is limited by external focusing $K < (\sigma_0 a/2L)^2$ **where K is the perveance (proportional to line charge density over beam Voltage), a is the average beam radius and L is the half-lattice period.**

Velocity tilt $\Delta v/v < \sim$ 0.3 for electrostatic quads **(larger for magnetic quads) to avoid mismatches at head and tail of beam, and to ensure tail radius within pipe and head σ_0 within limit)**

Volt-seconds per meter $(dV/ds)\, l/v_0$ <~ 1.5-2.0 V-s/m **(for "reasonable" core sizes)**

Voltage gradient dV/ds < ~ 1-2 MV/m **(to avoid breakdown in gaps)**

Sources of non-linearity and mismatch are well defined

Sources of non-linearities

- External focusing magnets
- Space-charge
- Multiple-beam effects

Sources of mismatch

- Accelerator imperfections
  - Quad strength and placement errors
  - Acceleration waveform errors
  - Bend strength errors
- Velocity tilt

Simulations give reliable and definitive tolerances on each source

Several potential instabilities have been investigated in HIF drivers

Temperature anisotropy instability

After acceleration $T_{||} << T_{\perp}$, internal beam modes are unstable; saturation occurs when $T_{||} \sim T_{\perp}/3$

Longitudinal resistive instability

Module impedance interacts with beam, amplifying space-charge waves that are backward propagating in beam frame

Beam break-up (BBU) instability

High frequency waves in induction module cavities interact transversely with beam

Beam-plasma instability

Beam interacts with residual gas in target chamber

All of these instabilities have known analytic linear growth rates, which constrain the accelerator design (to ensure minimal growth or benign saturation).

M. de Hoon studied a final current pulse that is flat with parabolic ends using the HERMES code

15 ns final pulse duration

The initial tilt on the beam is about 4% (compare to ~30% at the beginning of the accelerator)

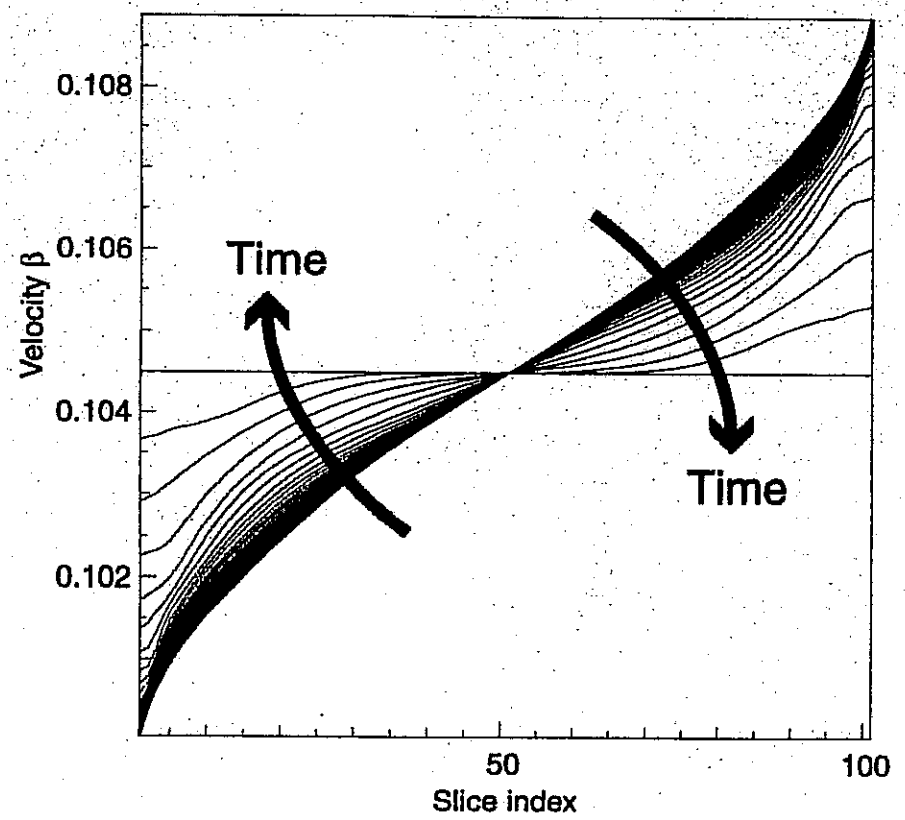

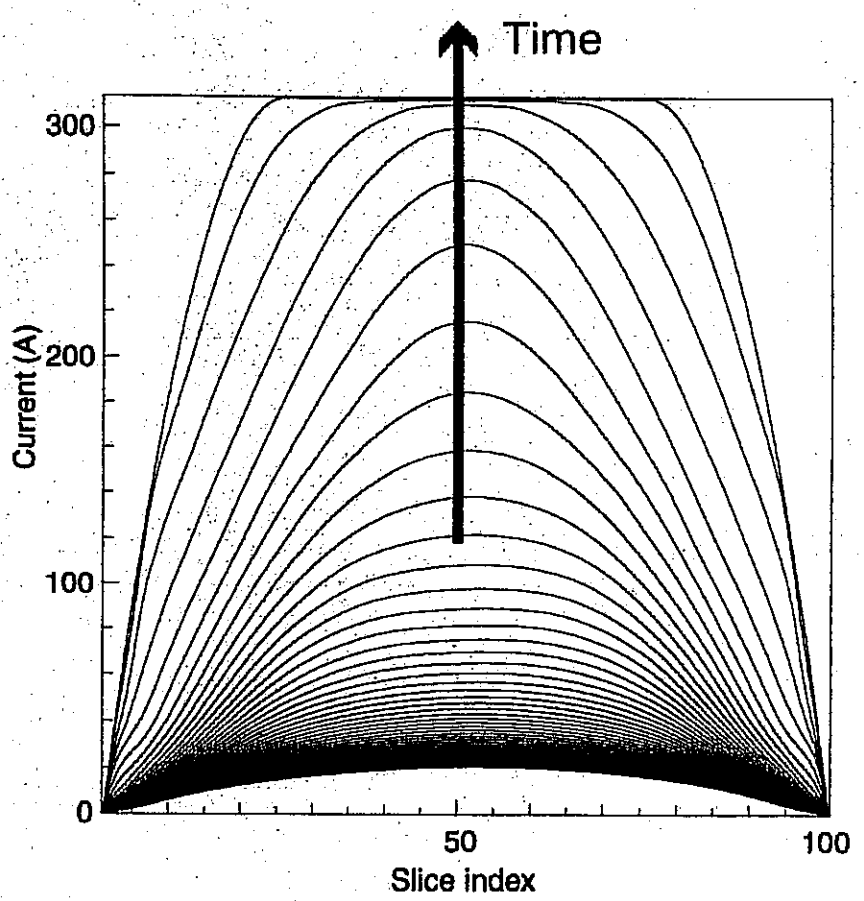

Although the final beam profile is flat, it is parabolic for most of the drift compression

Drift compression section is designed by running code first backwards from target, then forwards after rematching

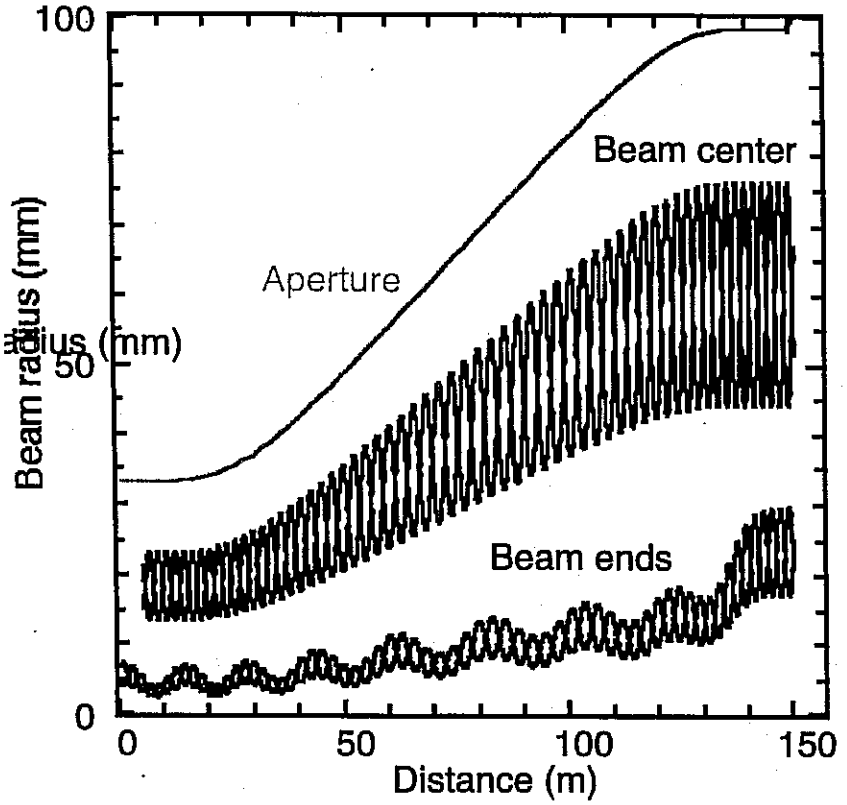

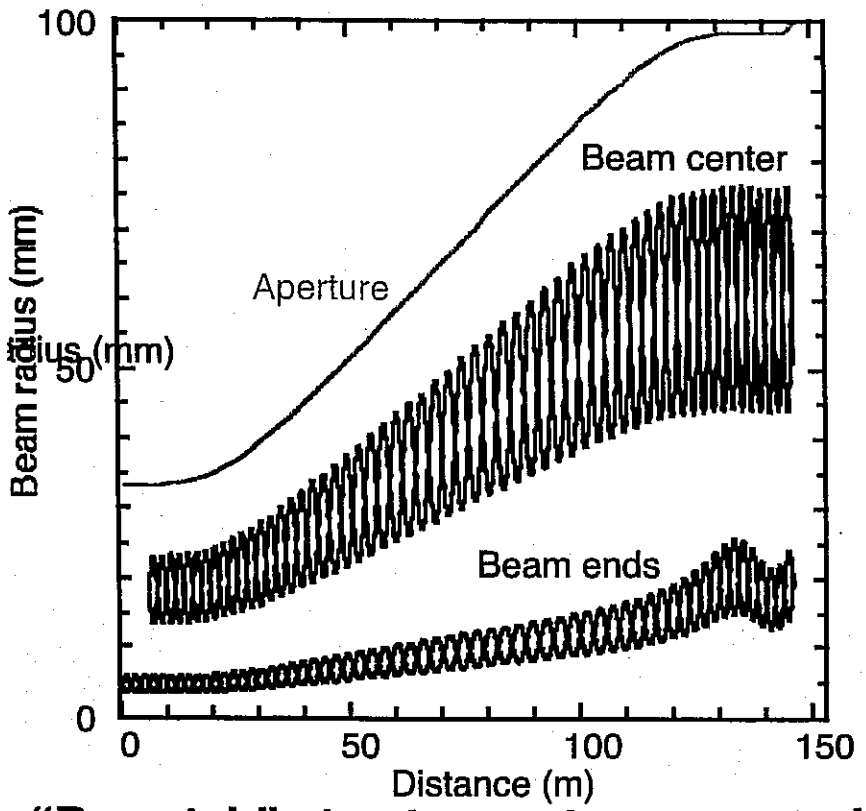

Begin with a desired 20ns, constant-energy pulse at end of compression, track backwards, design lattice for central slice; beam end becomes mismatched early on

"Rematch" at entrance to compression section, by adjusting a,a',b,b'; then track forward

A solenoid focus option leads to a low V, high current modular driver with advantageous development path

Pulse energy ~ 6.7 MJ

V~ 200-300 MV: T~ 2.5 GeV Xe^{+8} ions or T ~ 200 MeV for Ne^{+1}

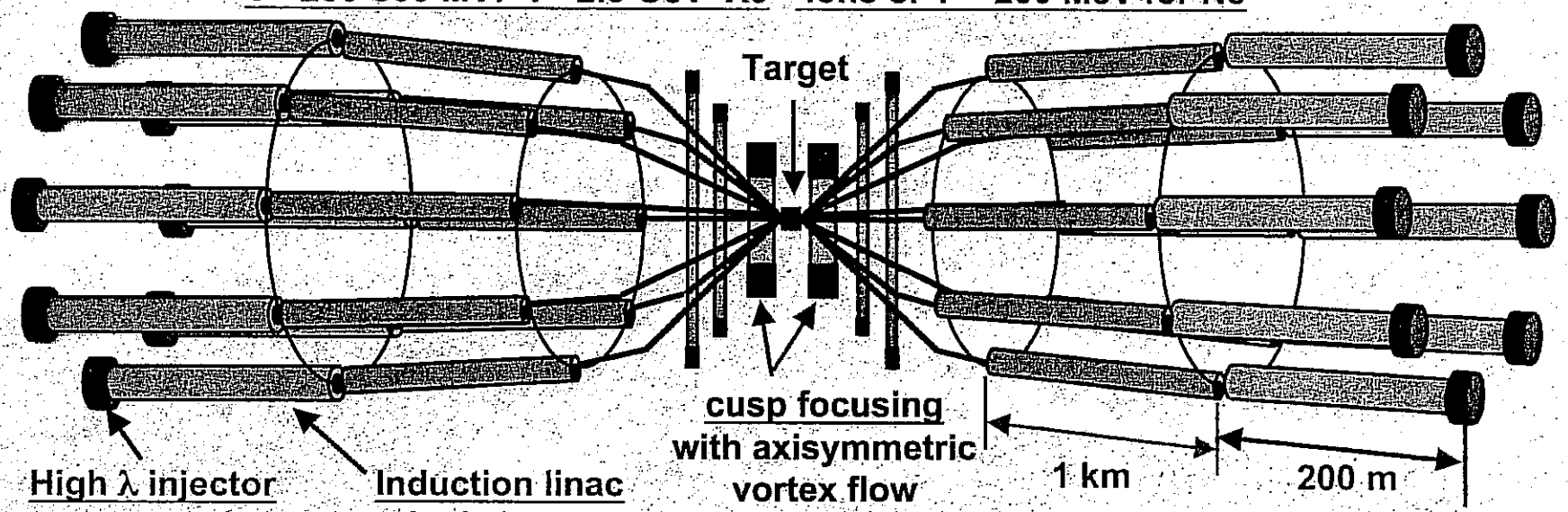

High λ injector

Merging beamlet source/injector

or

accel/decel injector

Induction linac

single beams

r_p ~ 15 cm

B_s ~ 9T

I ~ 6.7 kA

T ~ 2.5 GeV

Δt ~ 100 ns

double pulsed for foot and main pulses

cusp focusing

with axisymmetric vortex flow

or

adiabatic plasma lense assisted pinch with cross-jet flow. liquid walls

Neutralized drift compression

Δv/v ~ 0.01

(no space charge stagnation)

Summary of Current Limits From Different Focusing Methods

Einzel Lens

$$Q_{max} \cong \frac{3\pi^2}{\gamma}\left(\frac{q\phi_0}{m v_0^2}\right)^2\left(\frac{r_b}{L}\right)^2$$

Solenoids

$$Q_{max} = \left(\frac{\omega_c r_b}{2\gamma\beta c}\right)^2$$

Quadrupole Focusing

$$Q_{max} \cong \frac{\eta\phi_0}{2\pi}\left(\frac{\sin\frac{\eta\pi}{2}}{\frac{\eta\pi}{2}}\right)\left[\frac{B r_b}{[B\rho]}\left[\frac{r_b}{r_p}\right] \quad \frac{2qV_q}{\gamma m v_z^2}\left[\frac{r_b^2}{r_p^2}\right]\right]$$

MAGNETIC

Electric

For Non-Relativistic Beams

$$\lambda_{max} \propto \frac{Q_0^2}{V} \qquad \lambda_{max} \propto \frac{q}{m} B^2 r_p^2 \qquad \lambda_{max} \propto \begin{cases} B, V^{1/2} r_p \\ V_q \end{cases}$$

Note
Q_0 = Voltage between Einzel lenses
V_q = Voltage on a quad relative to ground
V = particle energy / q

The HYLIFE-II Ion beam-driven power plant is shown with a two-end target, illustrated from two sides and a linear heavy-ion induction driver

The liquid wall protection including beam ports is provided by pumping molten salt (Flibe) through the chamber

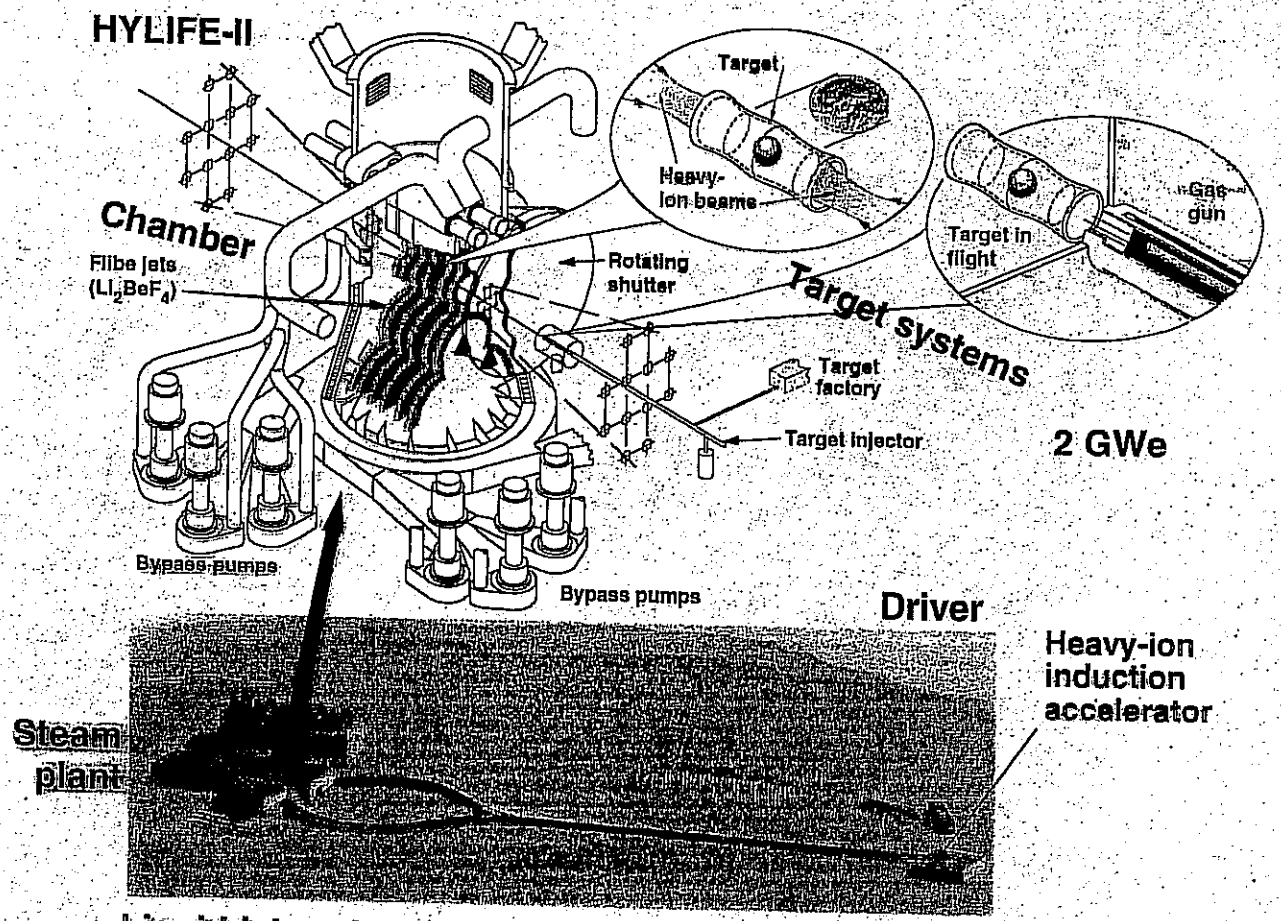

Liquid-jet protected fusion chambers for long lifetime, low cost, and low environmental impact

05-00-1194-3846U
16RWM/gbh

10/7/98

The First Wall Protected by Neutron-thick Molten Salt FLiBe,

FLiBe is a low Z salt ⇒ low activation ⇒ Green fusion energy

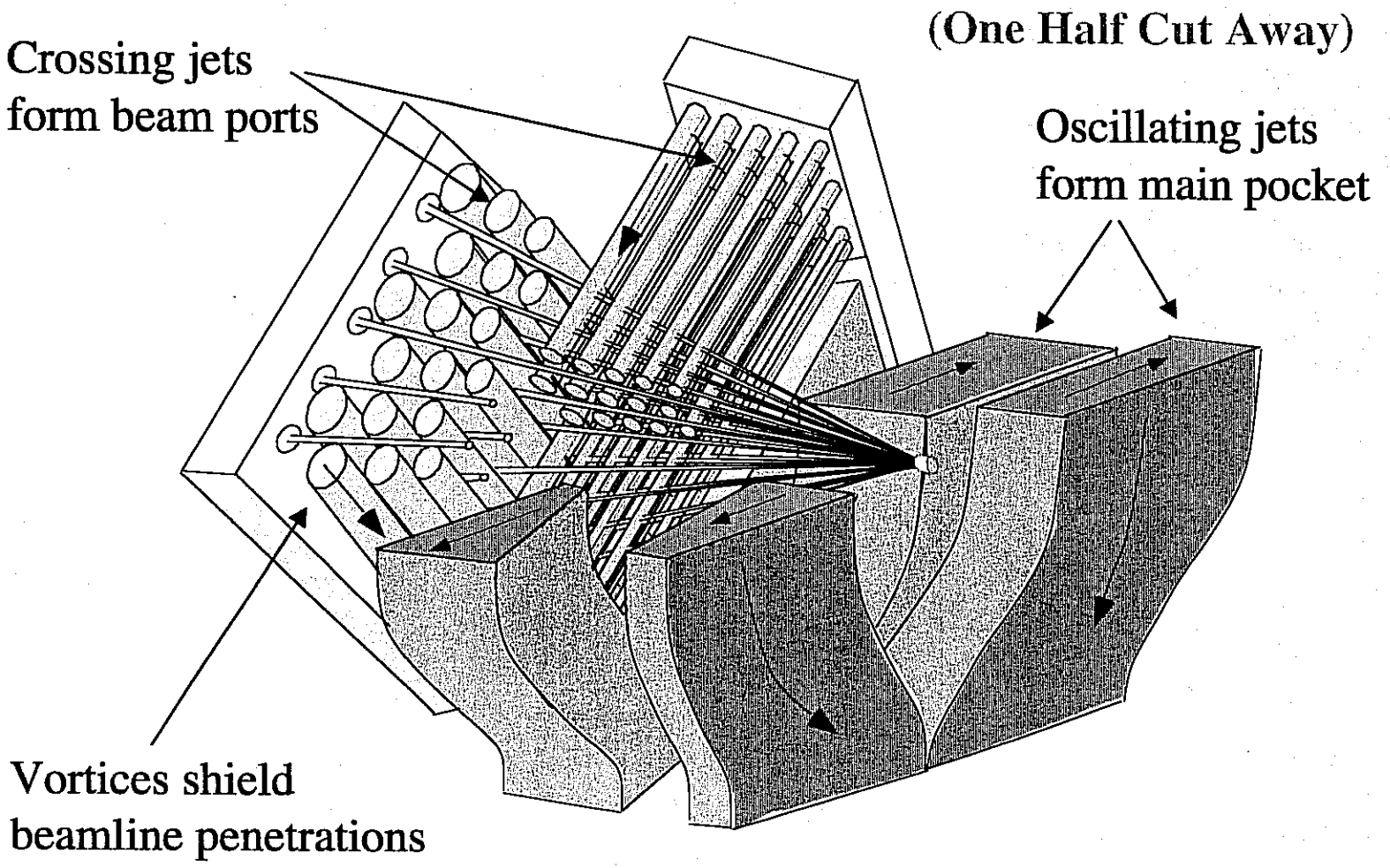

A number of final focus options are being considered for HIF applications

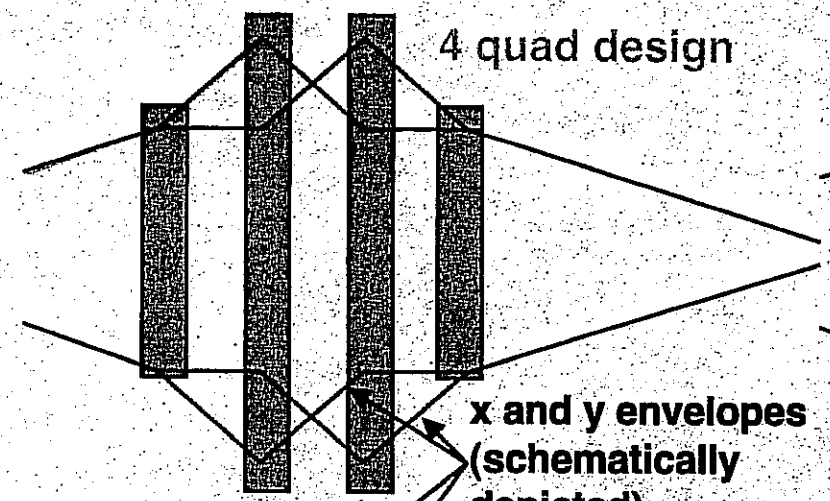

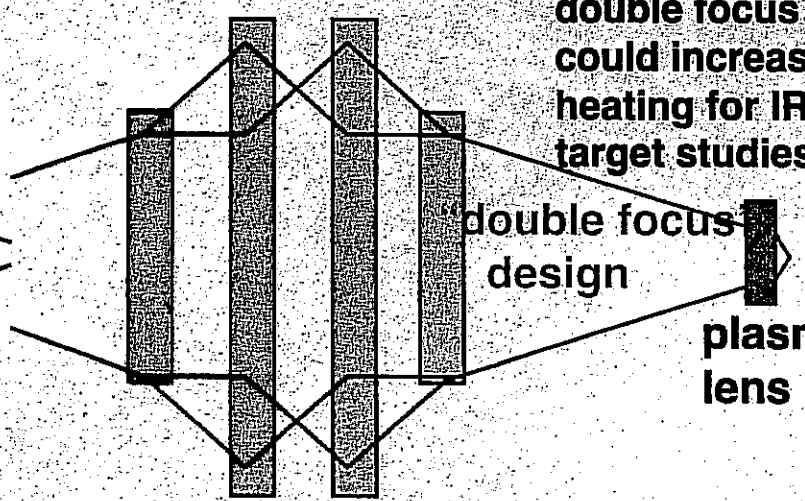

double focus design could increase spot heating for IRE target studies

x and y envelopes (schematically depicted)

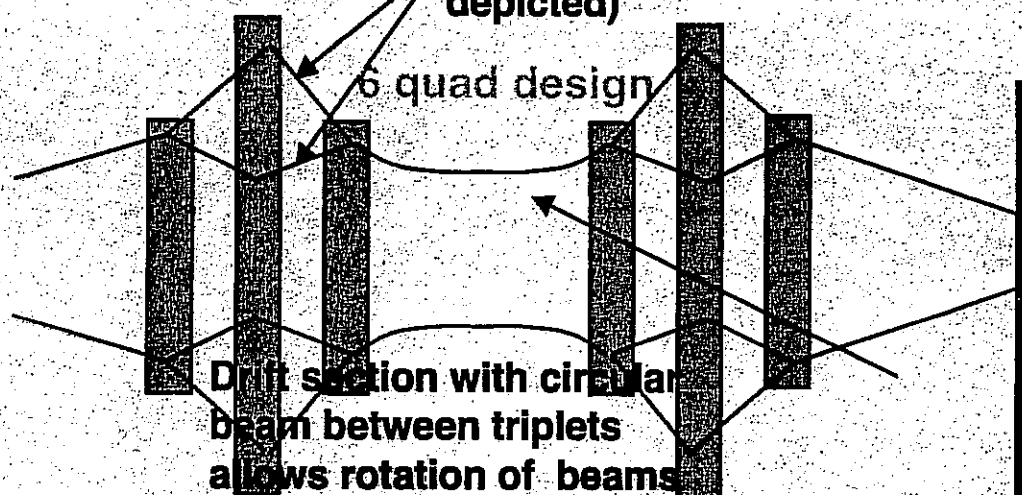

Drift section with circular beam between triplets allows rotation of beams or insertion of bend

Solenoid or cusp focusing is being considered for modular drivers:

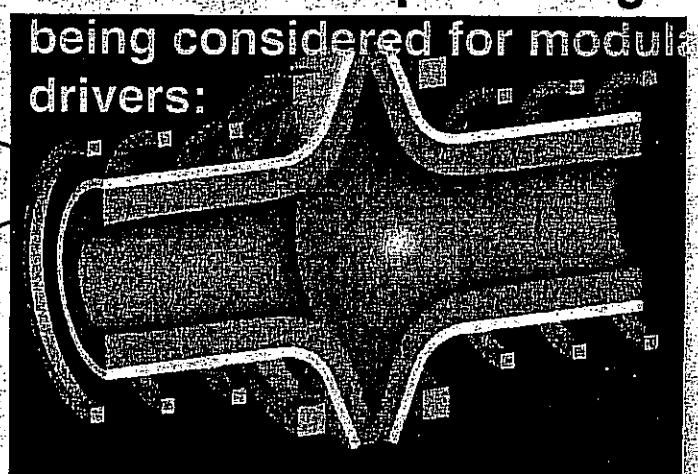

ESTIMATING SPOT SIZE

$$r_x'' + \frac{(\gamma_b \beta_b)'}{\gamma_b \beta_b} r_x + K_x r_x - \frac{2Q}{r_x + r_y} - \frac{\epsilon_x^2}{r_x^3} = 0$$

$$r_y'' + \frac{(\gamma_b \beta_b)'}{\gamma_b \beta_b} r_y + K_y r_y - \frac{2Q}{r_x + r_y} - \frac{\epsilon_y^2}{r_y^3} = 0$$

IN CHAMBER: NO EXTERNAL FOCUSING, NO ACCELERATION AND BEAM IS OFTEN CIRCULAR (BY DESIGN)

$$\Rightarrow K_x = K_y = (\gamma_b \beta_b)' = 0 \quad \& \quad r_x = r_y = r_b$$

$\Rightarrow$ ENVELOPE EQUATION IS:

$$r_b'' = \frac{Q}{r_b} + \frac{\epsilon^2}{r_b^3}$$

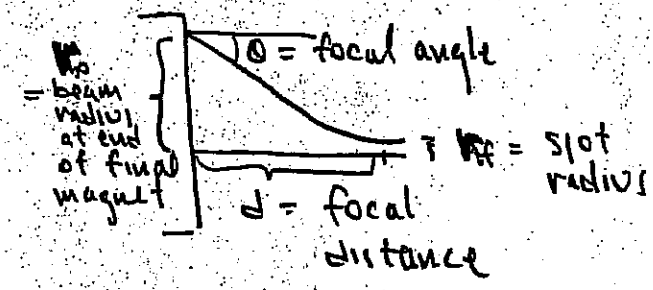

MULTIPLYING BY r_b' & INTEGRATING $\Rightarrow$

$$\frac{r_{bf}'^2}{2} - \frac{r_{bo}'^2}{2} = Q \ln \frac{r_{bf}}{r_{bo}} + \frac{\epsilon^2}{2 r_{bo}^2} - \frac{\epsilon^2}{2 r_{bf}^2}$$

Now $r_{bo}' \cong \theta$ $\quad r_{bf}$ = spot radius $\quad r_{bf} << r_{bo}$

$r_{bf}' = 0 \quad r_{bo} \cong d\theta$

$$\Rightarrow \boxed{\theta^2 \cong 2Q \ln\left(\frac{\theta d}{r_{bf}}\right) + \frac{\epsilon^2}{r_{bf}^2}}$$

FOR EMITTANCE DOMINATED SPOT: $r_{bf} = \frac{\epsilon}{\theta}$

"CHROMATIC ABERRATIONS" TEND TO BROADEN SPOT

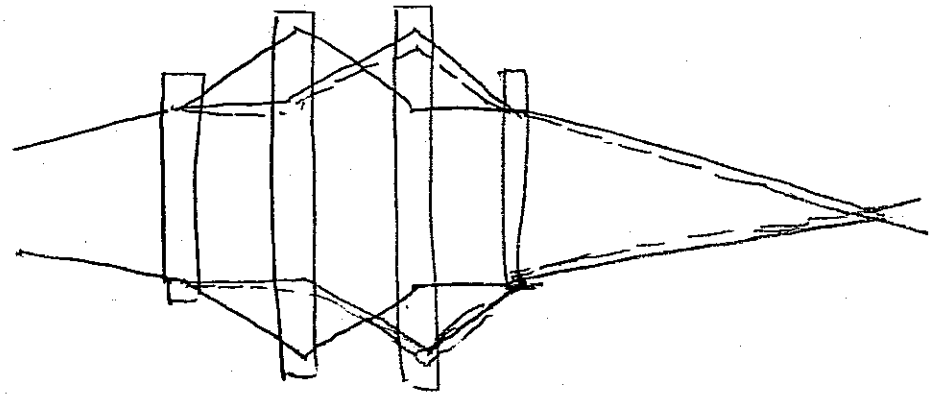

SINCE QUADRUPOLE MAGNET FOCUSING $\propto \frac{1}{V_z}$

(i.e. $x'' = \frac{qB'}{\gamma m v_z} x$) A SPREAD IN LONGITUDINAL VELOCITY GIVES RISE TO A BROADENING OF FINAL SPOT.

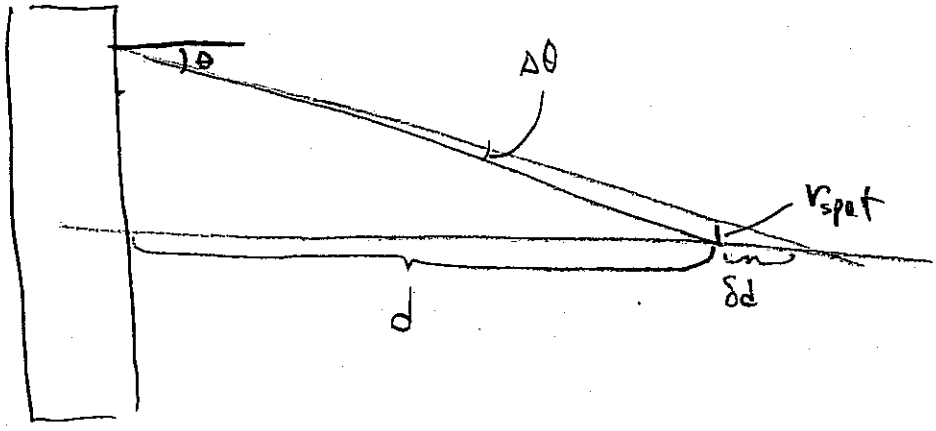

$$r_{spot} = \theta\,\delta d$$
$$= \theta \frac{dd}{d\theta} \frac{d\theta}{dp} \delta p$$
$$= \alpha\, \theta d \left(\frac{\delta p}{p}\right)$$

α = some constant depending on focal system

<u>HEURISTICALLY</u> THE CONTRIBUTION FROM CHROMATIC ABERRATIONS CAN BE WRITTEN

$$r_{chrom}^2 = \alpha^2 J^2 \left(\frac{\delta\gamma}{\gamma}\right)^2 \theta^2$$

where α depends on system, typically 4-8

$$r_{tot}^2 = r_{bf}^2 + r_{chrom}^2$$

DETAILED SIMULATIONS OR MOMENT CODE RESULTS REQUIRED TO FIX α.

We constructed moment models to study chromatic effects (through 2nd order) in final focus system

$$\frac{dp_x}{dt} = q(E_x + v_z B_y - v_y B_z)$$

Expand through 2nd order in x', y', $k_{\beta 0}x$, $k_{\beta 0}y$, $\delta p/p$

$$x'' + \left(\frac{1}{\gamma v_{z0}}\frac{d}{dz}(\gamma v_z)\right)x' = \frac{qB'}{\gamma m v_{z0}}x\left(1-\frac{\delta p}{p}\right) + \frac{q\lambda}{4\pi\varepsilon_0 m v_{z0}^2}\frac{(x-\bar{x})(1-\frac{2\delta p}{p})}{(\Delta x^2 + [\Delta x^2 \Delta y^2]^{1/2})}$$

The equation of motions can be written (where $\delta = \delta p/p$**) :**

$$\boxed{x'' = K_{xx}x + K_{xx1}x\delta \qquad y'' = K_{yy}y + K_{yy1}y\delta}$$

Here:

$$K_{xx} = \frac{B'}{[B\rho]_0} + \frac{Q}{2(\Delta x^2 + [\Delta x^2 \Delta y^2]^{1/2})} \qquad K_{yy} = \frac{-B'}{[B\rho]_0} + \frac{Q}{2(\Delta y^2 + [\Delta x^2 \Delta y^2]^{1/2})}$$

$$K_{xx1} = -\left[\frac{B'}{[B\rho]_0} + \frac{2Q}{2(\Delta x^2 + [\Delta x^2 \Delta y^2]^{1/2})}\right] \qquad K_{yy1} = -\left[\frac{-B'}{[B\rho]_0} + \frac{2Q}{2(\Delta y^2 + [\Delta x^2 \Delta y^2]^{1/2})}\right]$$

B' = **quadrupole gradient;** $[B\rho]$ = **Ion rigidity** $= p/q$; Q = **perveance** $= \frac{q\lambda}{2\pi\varepsilon_0 \gamma_0^3 m v_{z0}^2}$

We take averages of 2nd, 3rd,... order quantities, forming infinite set of 1st order ode's

$$\frac{d}{ds}\langle x^2\rangle = 2\langle xx'\rangle$$

$$\frac{d}{ds}\langle xx'\rangle = \langle x'^2\rangle + \langle xx''\rangle$$

$$= \langle x'^2\rangle + K_{xx}\langle x^2\rangle + \underline{K_{xx1}\langle x^2\delta\rangle}$$

$$\frac{d}{ds}\langle x'^2\rangle = 2\langle x'x''\rangle$$

$$= 2K_{xx}\langle xx'\rangle + \underline{2K_{xx1}\langle xx'\delta\rangle}$$

$$\frac{d}{ds}\langle x^2\delta\rangle = 2\langle xx'\delta\rangle$$

$$\frac{d}{ds}\langle xx'\delta\rangle = \langle x'^2\delta\rangle + \langle xx''\delta\rangle$$

$$= \langle x'^2\delta\rangle + K_{xx}\langle x^2\delta\rangle + \underline{K_{xx1}\langle x^2\delta^2\rangle}$$

$$\frac{d}{ds}\langle x'^2\delta\rangle = 2\langle x'x''\delta\rangle$$

$$= 2K_{xx}\langle xx'\delta\rangle + \underline{2K_{xx1}\langle xx'\delta^2\rangle}$$

...

$$\frac{d}{ds}\langle x^2\delta^n\rangle = 2\langle xx'\delta^n\rangle$$

$$\frac{d}{ds}\langle xx'\delta^n\rangle = \langle x'^2\delta^n\rangle + \langle xx''\delta^n\rangle$$

$$= \langle x'^2\delta^n\rangle + K_{xx}\langle x^2\delta^n\rangle + \underline{K_{xx1}\langle x^2\delta^{n+1}\rangle}$$

$$\frac{d}{ds}\langle x'^2\delta^n\rangle = 2\langle x'x''\delta^n\rangle$$

$$= 2K_{xx}\langle xx'\delta^n\rangle + \underline{2K_{xx1}\langle xx'\delta^{n+1}\rangle}$$

—— => term higher order by one

Infinite set of equations can be truncated, but are reliable over only finite distances

Two equivalent methods of truncation have been employed:

1. $\langle x^2\delta^2\rangle \sim \langle x^2\rangle\langle\delta^2\rangle$ and $\langle xx'\delta^2\rangle \sim \langle xx'\rangle\langle\delta^2\rangle$; or
2. Noticing that $\frac{1}{1+\delta} = 1-\delta+\delta^2+\ldots$ and $\frac{1}{1-\delta} = 1+\delta+\delta^2+\ldots$ thus,

$\frac{1}{1-\delta} - \frac{1}{1+\delta} = 2\delta + 2\delta^3 + \ldots$ also $\frac{\delta}{1+\delta} = 1 - \frac{1}{1+\delta}$

so that we may, to good approximation, write

$$\frac{d}{ds}\langle x^2\rangle = 2\langle xx'\rangle \qquad \frac{d}{ds}\langle xx'\rangle = \langle x'^2\rangle + K_{xx}\langle x^2\rangle + \frac{K_{xx1}}{2}\left[\left\langle\frac{x^2}{1-\delta}\right\rangle - \left\langle\frac{x^2}{1+\delta}\right\rangle\right] + O\left(x^2\delta^3\right)$$

$$\frac{d}{ds}\langle x'^2\rangle = 2K_{xx}\langle xx'\rangle + K_{xx1}\left[\left\langle\frac{xx'}{1-\delta}\right\rangle - \left\langle\frac{xx'}{1+\delta}\right\rangle\right] + O(xx'\delta^3)$$

$$\frac{d}{ds}\left\langle\frac{xx'}{1+\delta}\right\rangle = \left\langle\frac{x'^2}{1+\delta}\right\rangle + K_{xx}\left\langle\frac{x^2}{1+\delta}\right\rangle - K_{xx1}\left\langle\frac{x^2}{1+\delta}\right\rangle + K_{xx1}\langle x^2\rangle \qquad \frac{d}{ds}\left\langle\frac{x^2}{1+\delta}\right\rangle = 2\left\langle\frac{xx'}{1+\delta}\right\rangle$$

$$\frac{d}{ds}\left\langle\frac{x'^2}{1+\delta}\right\rangle = 2K_{xx}\left\langle\frac{xx'}{1+\delta}\right\rangle + 2K_{xx1}\langle xx'\rangle - 2K_{xx1}\left\langle\frac{xx'}{1+\delta}\right\rangle$$

Truncated set of equations forms closed set.

both methods give nearly identical results for $\langle\delta^2\rangle$ in the regime of interest; similar equations for $\langle x^2/(1-\delta)\rangle$, $\langle xx'/(1-\delta)\rangle$, $\langle x'^2/(1-\delta)\rangle$, and the same set for y; 18 equations total.

Comparison of moment equations with Particle-in-Cell (WARP[1]) simulations (1% velocity spread)

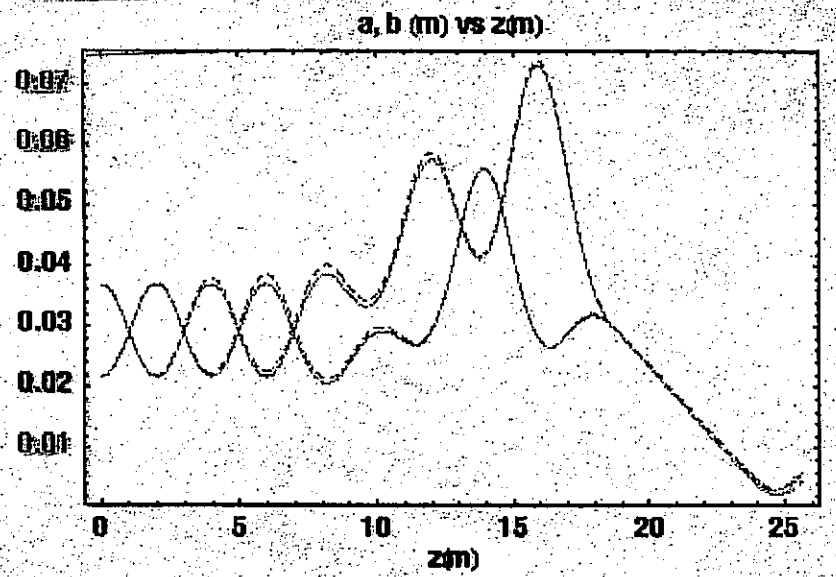

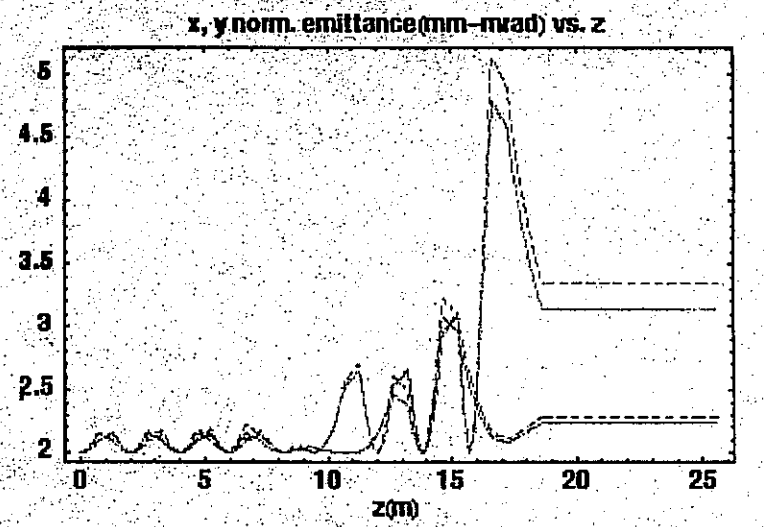

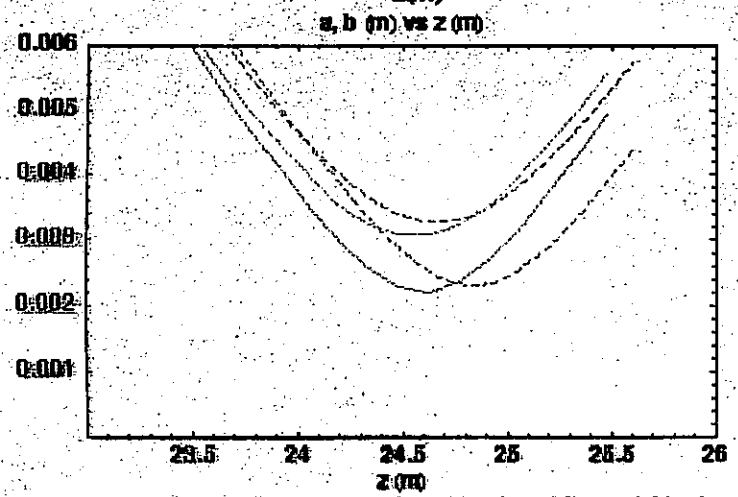

Particle simulations:
Dashed, red (x) and blue (y)
Initial distribution: KV

Moment calculations:
Solid, magenta (x), and aqua (y)

Comparison of moment equations with PIC simulations (WARP) -- no velocity spread

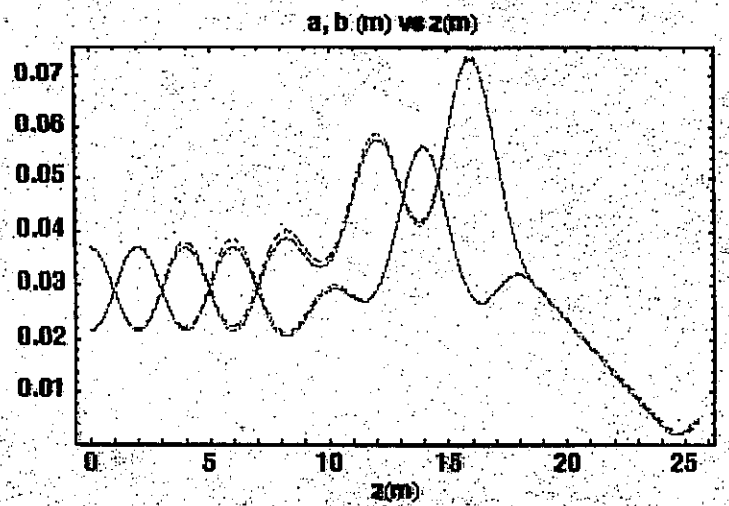

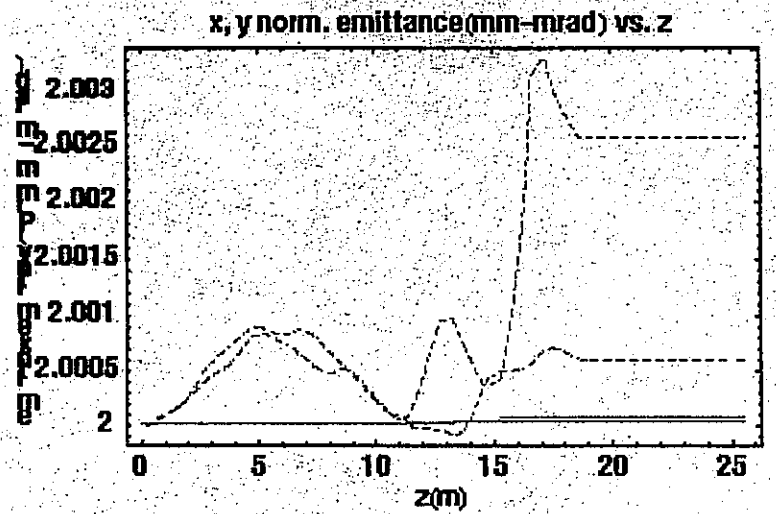

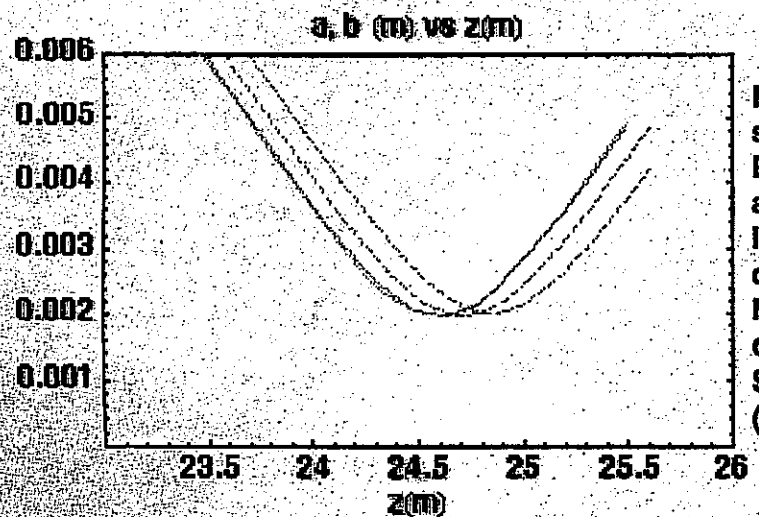

Particle simulations: Dashed, red (x) and blue (y)
Initial distribution: KV
Moment calculations: Solid, magenta (x), and aqua (y)

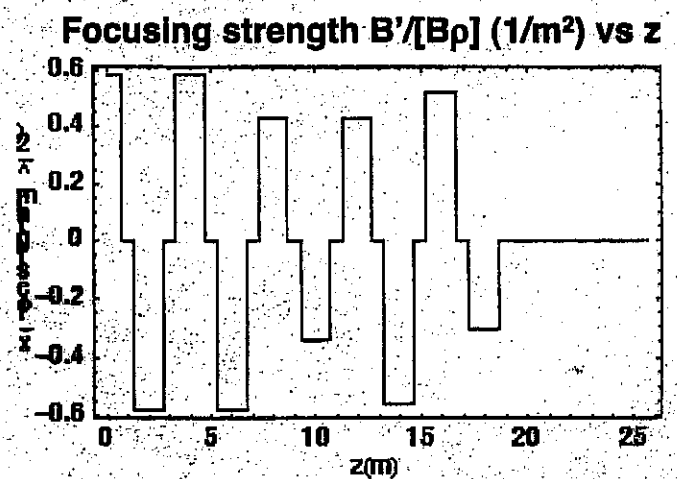

BEAM PHYSICS RESEARCH AT LLNL/LBNL/PPPL (THE HEAVY ION FUSION SCIENCE VIRTUAL NATIONAL LAB) FOCUSES ON TWO MAIN EXPERIMENTS:

1. "HIGH BEAM BRIGHTNESS" ON THE HIGH CURRENT EXPERIMENT (HCX)
   - ELECTRON CLOUD
   - MAXIMUM TRANSPORTABLE CURRENT

2. NEUTRALIZED DRIFT COMPRESSION AND FOCUSING EXPERIMENTS (NDCX-1)
   - NEUTRALIZED DRIFT COMPRESSION
   - NEUTRALIZED FINAL FOCUS
   - PULSE LINE ION ACCELERATOR

The High Current Experiment (HCX) is exploring beam transport limits

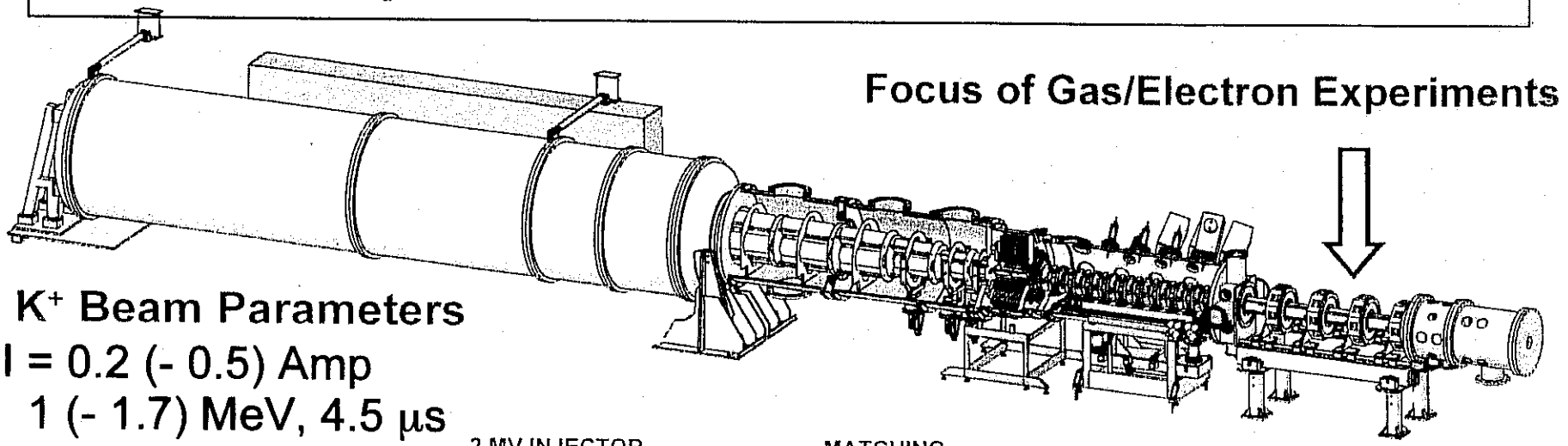

K^+ Beam Parameters
I = 0.2 (- 0.5) Amp
1 (- 1.7) MeV, 4.5 μs

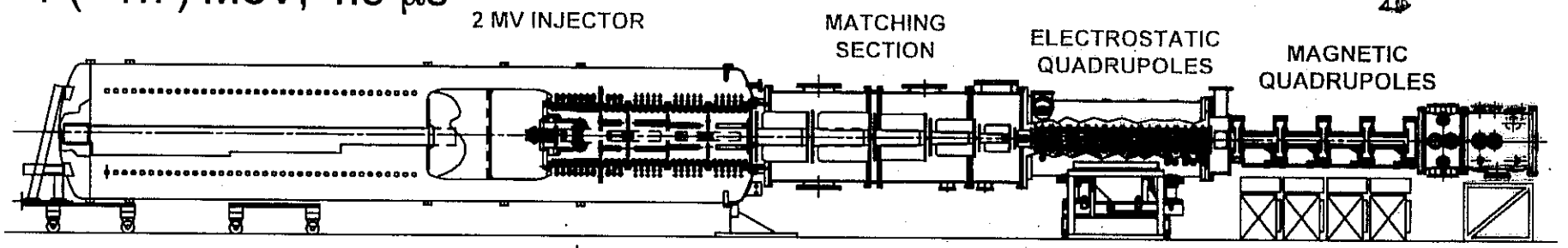

4 magnetic quadrupoles; many diagnostics

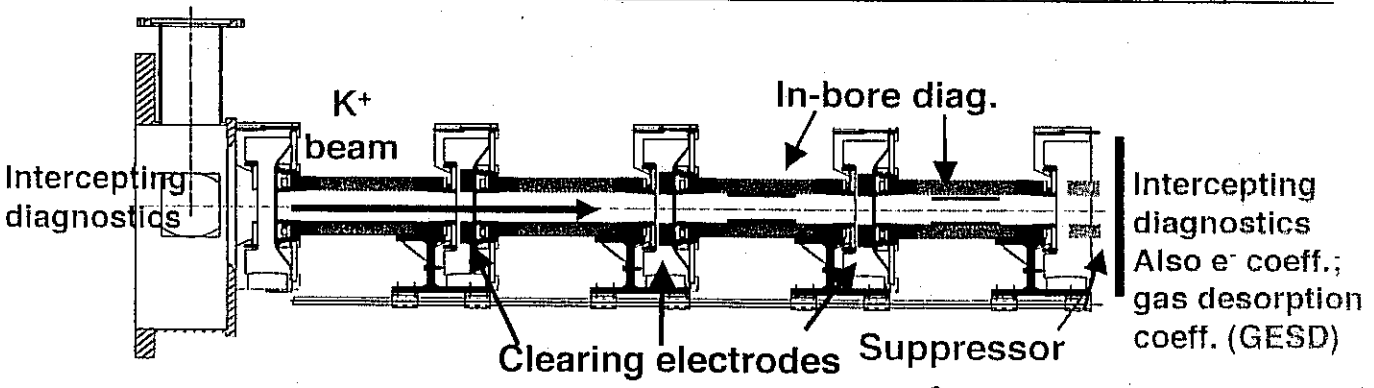

Neutralized Transport Experiment investigated physics of neutralized focusing

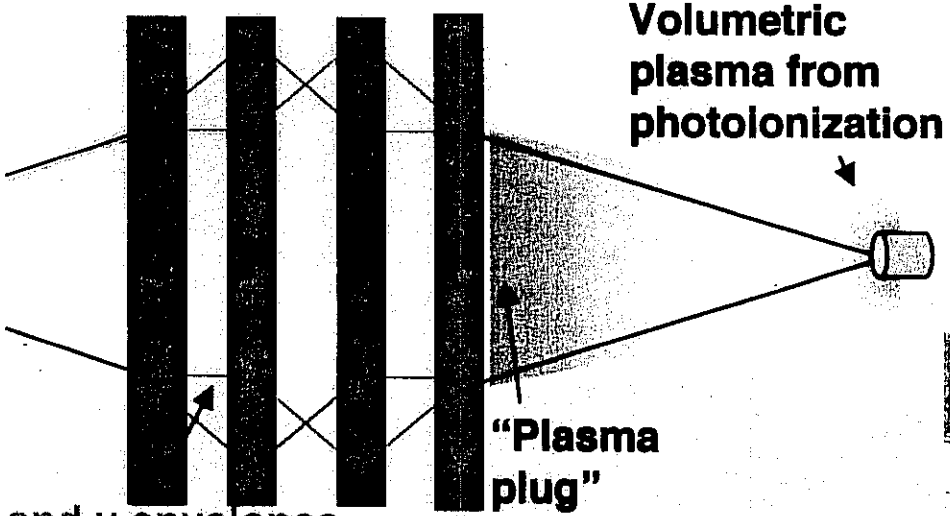

x and y envelopes (schematically depicted)

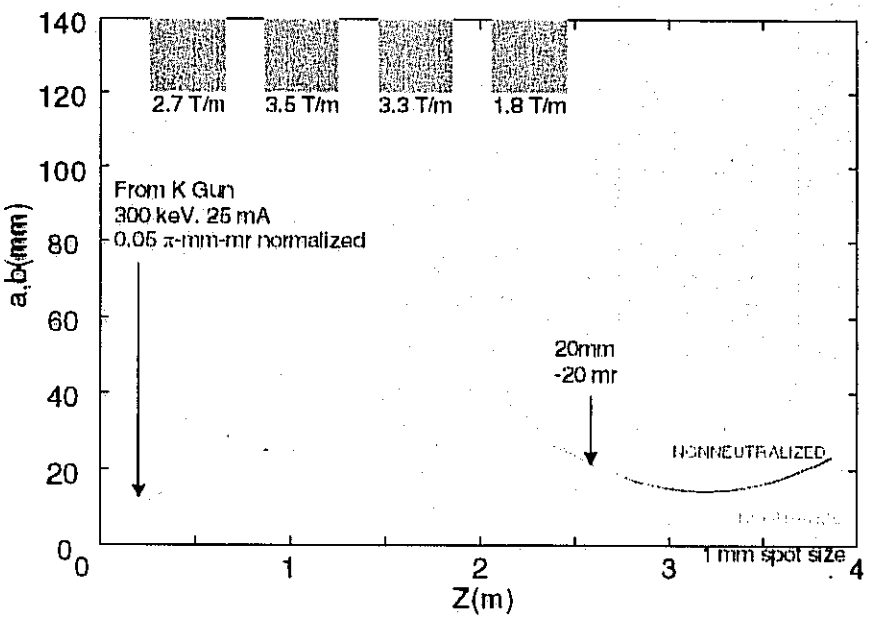

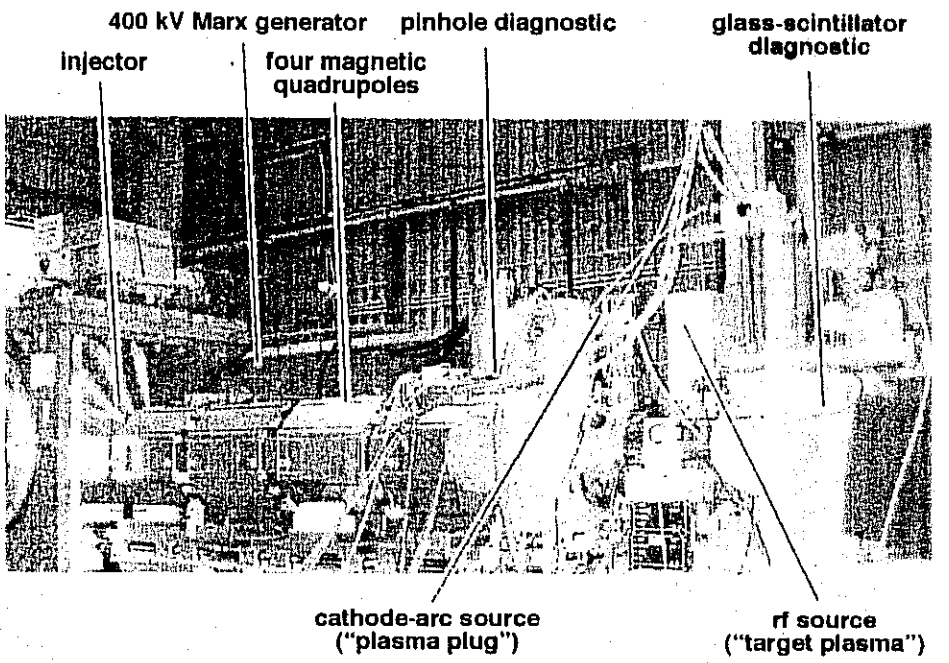

300 keV K+ ions at 25 mA

2004

Measurements on the Neutralized Transport Experiment (NTX) demonstrate achievement of smaller transverse spot size using volumetric plasma

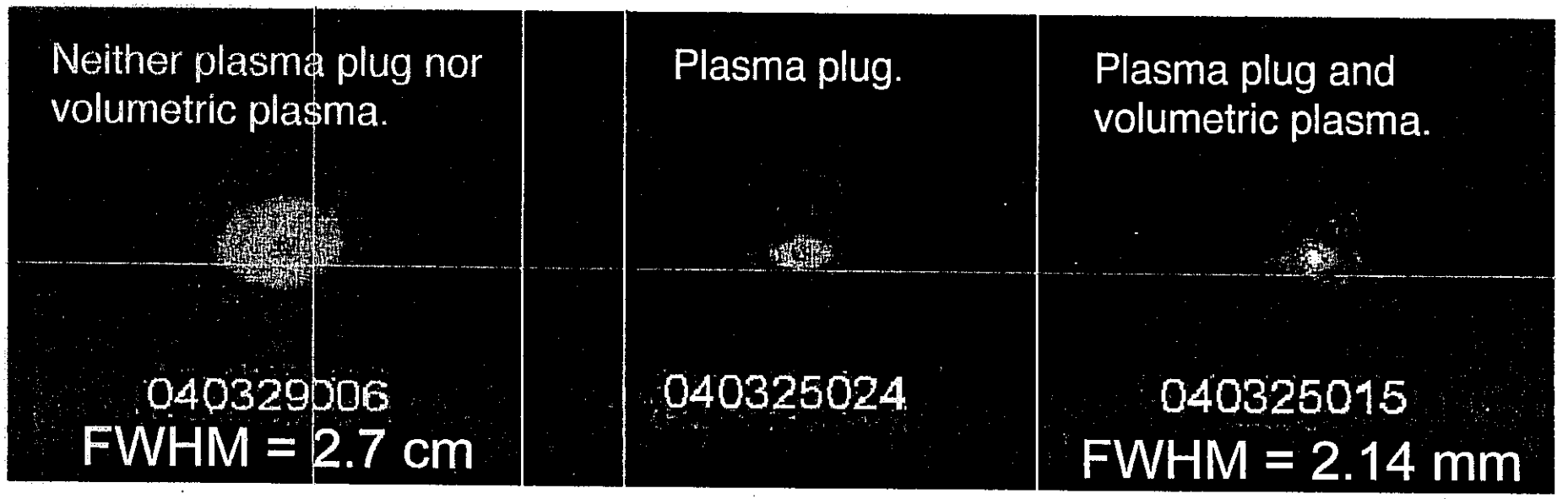

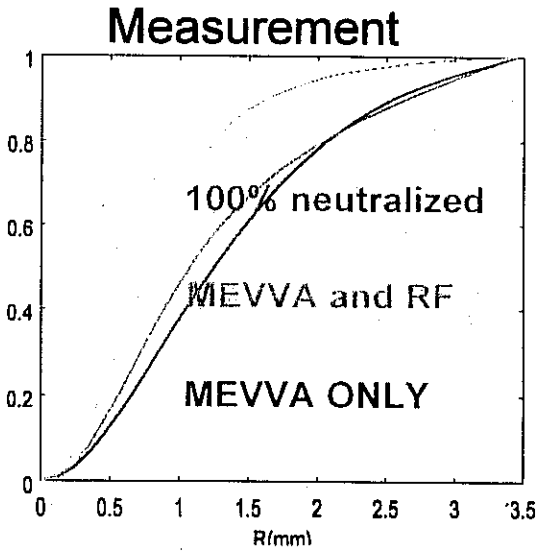

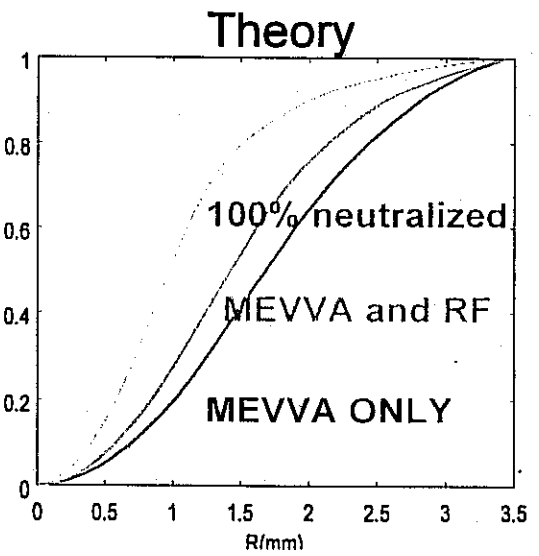

Neutralized drift compression experiment (NDCX) - 300 keV K+ ions at 25 mA

Tiltcore waveform

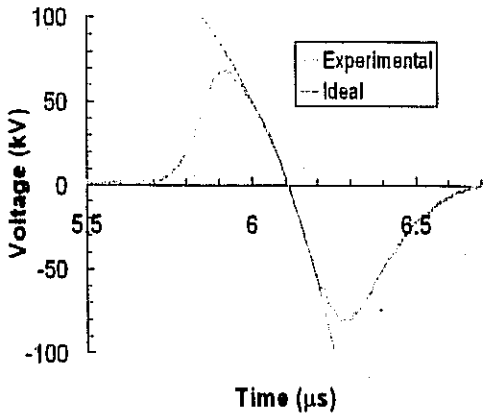

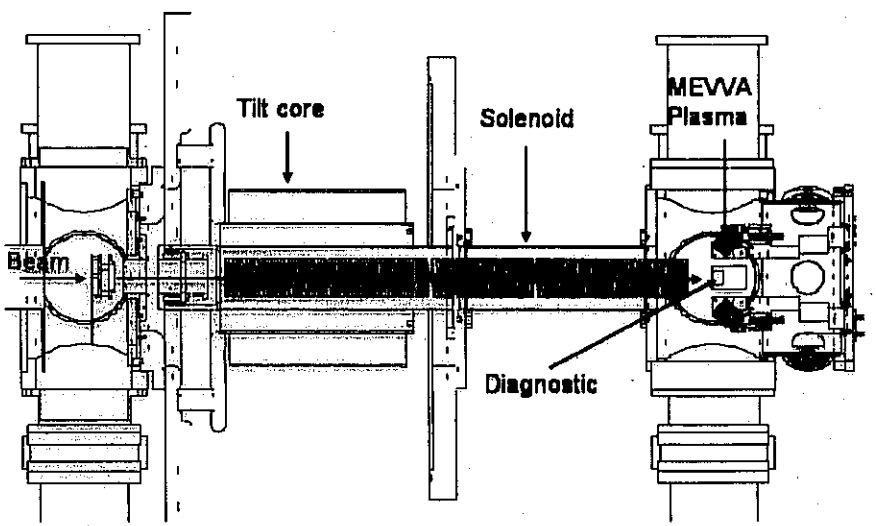

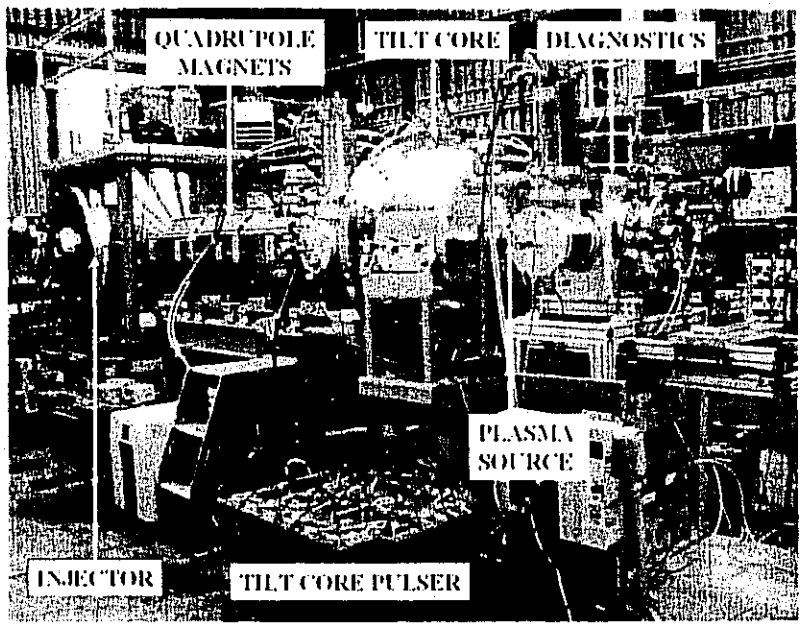

50 Fold Beam compression achieved in neutralized drift compression experiment

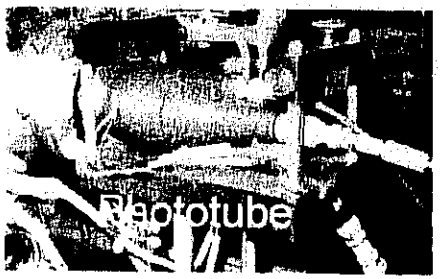

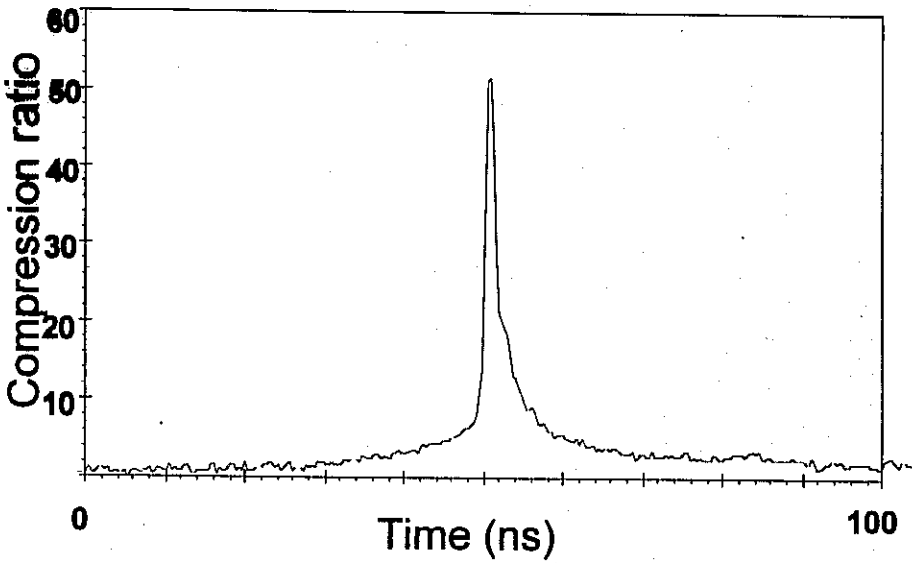

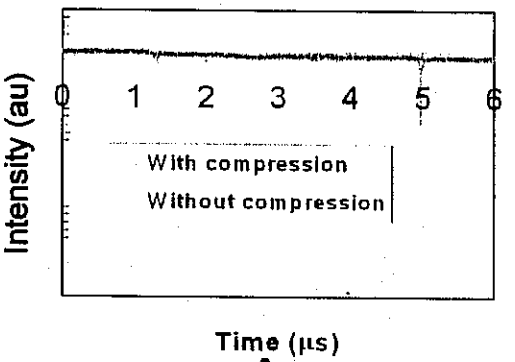

Optical data

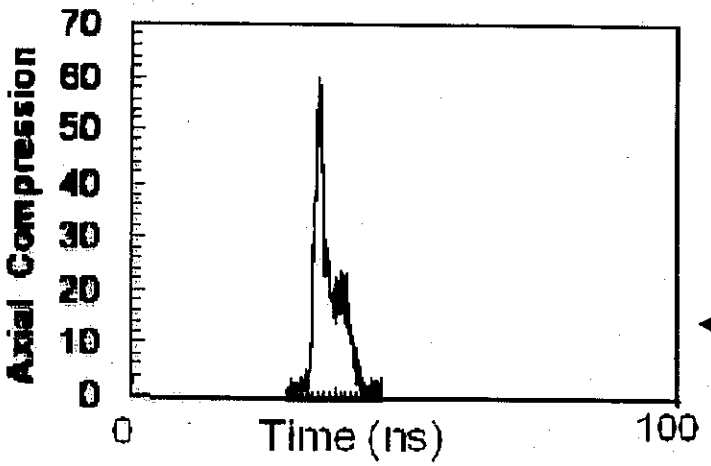

LSP simulation

Corroborating data from Faraday cup

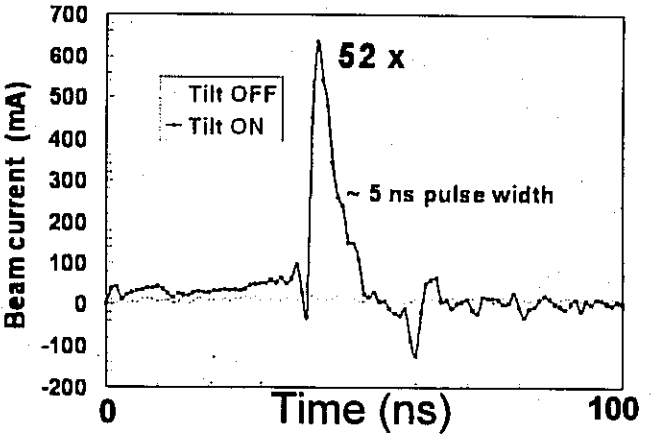

P.K. Roy et al, PRL, **95**, 234801, 2 Dec. 2005

NDCX-I: A series of experiments towards HEDP (NDCX-II)

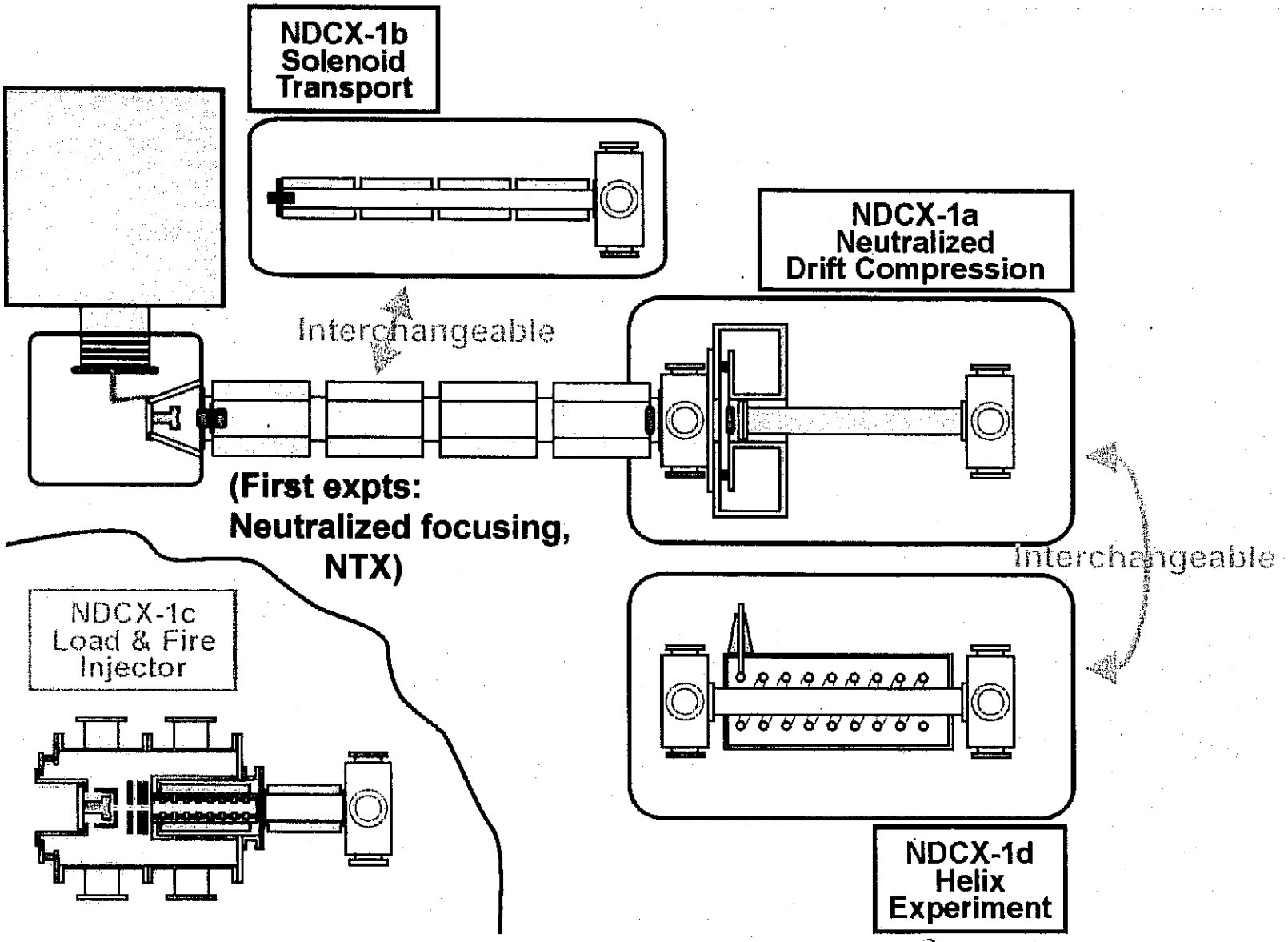
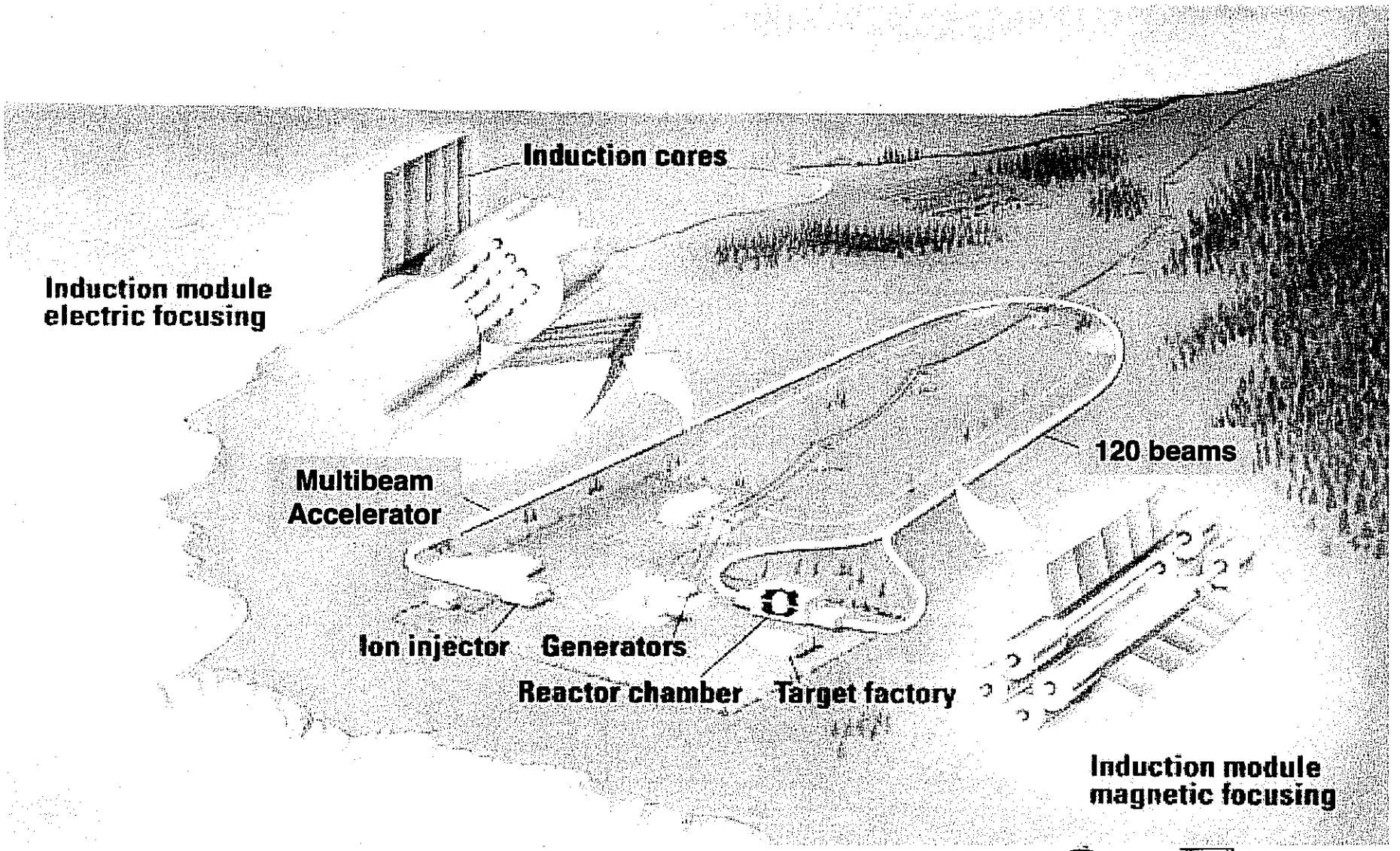
Artist's Conception of an HIF Power Plant on a few km^2 site